DYNAMIC FORCE MEASUREMENT TECHNIQUES IN SPLIT HOPKINSON PRESSURE BAR TESTING OF LOW ACOUSTIC IMPEDANCE MATERIALS USED AS ARMOR INTERLAYER MATERIALS

A Thesis Submitted to
the Graduate School of Engineering and Sciences of
İzmir Institute of Technology
in Partial Fulfillment of the Requirements for the Degree of

MASTER OF SCIENCE

in Mechanical Engineering

by
Ali Kıvanç TURAN

July 2012
İZMİR

We approve the thesis of **Ali Kıvanç TURAN**

Examining Committee Members:

Assoc. Prof. Dr. Alper TAŞDEMİRCİ
Department of Mechanical Engineering
İzmir Institute of Technology

Assoc. Prof. Dr. Bülent Murat İÇTEN
Department of Mechanical Engineering
Dokuz Eylül University

Assist. Prof. Dr. Engin ÖZÇİVİCİ
Department of Mechanical Engineering
İzmir Institute of Technology

05 July 2012

Assoc. Prof. Dr. Alper TAŞDEMİRCİ
Supervisor, Department of Mechanical Engineering
İzmir Institute of Technology

Prof. Dr. Mustafa GÜDEN
Co-Supervisor, Department of Mechanical Engineering
İzmir Institute of Technology

Prof. Dr. Metin TANOĞLU
Head of the Department of Mechanical Engineering

Prof. Dr. R. Tuğrul SENGER
Dean of the Graduate School of Engineering and Sciences

ACKNOWLEDGEMENTS

First and foremost, I would like to express my deepest gratitude to my supervisor, Associate Prof. Dr. Alper TAŞDEMİRCİ, for his mental support and guidance through this study with his supportive behavior. His approach to overcome the problems encountered has encouraged me to fulfill this study. I also would like to thank to my co-advisor Prof. Dr. Mustafa GÜDEN with his valued support throughout the study. I would like to thank İ. Kutlay ODACI, Ali KARA and Cenk KILIÇASLAN for their physical and mental support throughout the study as brothers rather than colleagues. I also would like to thank to Umut SAVACI, Doğuş ZEREN and Yiğit ATTİLA for their motivational behaviors.

This study, as the ones before, is dedicated to my beloved family. Firstly, I would thank to my father who has been and will be my idol, Yavuz Selim TURAN, for his absolute guidance through my entire life. I gratefully thank to my mother, Hülya TURAN, for raising me with her tender heart. Her innovative vision and aims in life enhanced my point of view in every aspect. I also would like to thank to my elder brother, O. Onur TURAN, for being caring and supportive in every nerve wracking situation with his admirable sense of humor.

Finally, I would like to thank my girlfriend Selin SARI for her patience and emotional support.

ABSTRACT

DYNAMIC FORCE MEASUREMENT TECHNIQUES IN SPLIT HOPKINSON PRESSURE BAR TESTING OF LOW ACOUSTIC IMPEDANCE MATERIALS USED AS ARMOR INTERLAYER MATERIALS

Gore™ Polarchip™ heat insulating Teflon and Dow Chemicals™ Voracor CS Polyurethane were characterized in this study by conducting compression tests at various strain rates. Quasi-static compression tests were done with a Shimadzu AG-X conventional test machine while two different modified Split Hopkinson Pressure Bar (SHPB) systems were used for dynamic compression tests. Since dynamic testing of soft materials with classical SHPB is problematic due to low signal levels and relatively higher signal to noise ratio, impact end of transmitter bar was modified with insertion of piezoelectric force transducers through the SHPB tests of Teflon, thus enabling the direct measurement of force on specimen. High strain tests of Polyurethane involved oscillations in both incident and transmitter bar signals. To overcome this, EPDM rubber pulse shaper was used through the SHPB tests of Polyurethane. Experimental results were used in numerical study as material model parameters and SHPB tests of both materials were simulated in LS-DYNA. Experimental study concluded strong strain rate dependency in both Teflon and Polyurethane, depicting an increase in maximum stress with the increase in strain rate. Numerical study showed a good correlation with experiments in terms of bar stresses and damage behavior of specimens, offering a solution to more complex problems that can be encountered in future studies.

ÖZET

ZIRH ARA YÜZEY MALZEMESİ OLARAK KULLANILAN DÜŞÜK AKUSTİK EMPEDANSLI MALZEMELERİN SPLİT HOPKİNSON BASINÇ BARI TESTİNDEKİ DİNAMİK KUVVET ÖLÇÜM TEKNİKLERİ

Bu çalışmada Gore™ Polarchip™ Teflon ve Dow Chemicals™ Voracor CS Poliüretan değişen deformasyon hızlarında basma testi yapılarak karakterize edilmiştir. Yarı-statik basma testleri için Shimadzu AG-X konvansiyonel test cihazı kullanılırken dinamik basma testleri için iki adet Split Hopkinson Basınç Barı (SHBB) sistemi kullanılmıştır. Yumuşak malzemelerin SHBB testlerinde düşük sinyaller ve göreceli olarak yüksek sinyal/gürültü oranları gözlendiği için, Teflon'un dinamik testlerinde ileten çubuğun numune tarafına piezoelektrik kuvvetölçerler eklenmiş ve bu sayede direkt olarak kuvvet ölçümü yapılmıştır. Poliüretanın yüksek hızlı deformasyon testlerinde çubuklardan alınan sinyallerde osilasyon görülmüştür. Bu durumun önlenmesi için Poliüretanın SHBB testlerinde EPDM kauçuktan sinyal şekillendiriciler kullanılmıştır. Deneylerden elde edilen sonuçlar nümerik çalışmada malzeme modeli parametreleri olarak kullanılmış ve bu malzemelerin SHBB testleri LS-DYNA'da taklit edilmiştir. Deneysel çalışma iki malzemede de güçlü bir deformasyon hızı etkisi olduğunu göstermiş, deformasyon hızının artması ile maksimum gerilmenin arttığını göstermiştir. Nümerik çalışma ise çubuk gerilmeleri ve numunelerin hasar alması bakımından deneysel çalışma ile uyumluluk göstermiş, gelecekte yapılacak daha karmaşık çalışmalarda bir çözüm sunmuştur.

TABLE OF CONTENTS

LIST OF FIGURES

Table **Page**

LIST OF TABLES

Table **Page**

CHAPTER 1

INTRODUCTION

1.1. Introduction

Since late 19th century, gun-fired projectiles have become a massive threat to mankind in war and peace times. Invention of antiaircraft guns, antitank rifles, portable and submachine guns have brought out the necessity of using protective equipment to reduce the number of casualties. In this manner, first defensive systems to increase protection against projectile threat included steel monolithic layers and increasing the thickness of steel was the main idea to increase safety [1-3]. However, development of newer weapons such as antitank missiles, shaped charges and hardened long rod penetrators have resulted in the defeat of conventional armor designs. In search of better protection, more efficient armor systems and protective equipment have been developed to lessen the damage initiated to crew and vehicle itself, increasing survivability against varying threats. For this purpose, ceramic front layer was included to the monolithic steel armor, aiming to erode the penetrator on the first microseconds of impact and reduce penetration by decreasing the kinetic energy of projectile due to friction on impact area. Backing plate was selected as either steel or composite to further absorb the kinetic energy of penetrator [4-6]. In addition to hard ceramic face, insertion of a low acoustic impedance interlayer also enhances the ballistic performance of multilayered armor systems. Different types of materials such as rubber, Teflon and aluminum foam were used as interlayer materials to distribute concentrated stress caused by impact of projectile and reduce the damage inflicted to backing plate [7-10].

When developing new armor systems, it is essential to use a laboratory oriented methodology as well as ballistic testing based on the method of trial-error. For this purpose, stress wave propagation in an interlayer material can be investigated by conducting Split Hopkinson Pressure Bar (SHPB) tests. SHPB testing may help to determine the stress wave propagation of either an individual layer [11] or all layers of an multilayered armor systems [12-14].

As a result of previous studies, an interlayer between hard ceramic face and steel/composite backing plate is essential to enhance ballistic performance. Polymeric foams with their low acoustic impedance allow those materials to lower the magnitude and rise time of stress wave transmitted as well as their weight advantage improves performance of areal density when compared to monolithic armors. Their relatively higher energy absorption capability also makes them a possible candidate to be used as an armor interlayer material [10]. Some of the recent studies focus on the feasibility of soft materials to be used in applications where shock or impact loading may occur. Thus, proper characterization of those materials and understanding the response of material to variability in loading is essential to have safer designs. Chen et al [15] have investigated the mechanical behavior of RTV 630 silicone rubber and Styrofoam at different strain rates. A conventional hydraulically driven test machine was used for low strain rates and a SHPB was occupied for high strain rate testing of selected materials. Classical SHPB was modified with X-cut quartz crystals added to the middle of transmitted bar, thus enabling the measurement of force directly. Experiments concluded that RTV630 silicone rubber and Styrofoam were found to be strain rate sensitive and modified split Hopkinson pressure bar was found to be three orders of magnitude as sensitive as a conventional SHPB.

Chen et al [16] have investigated the high strain rate compressive behavior of polyurethane foam with four different density values. Materials were tested from low to high strain rates to demonstrate the effect of strain rate. Quasi-static tests were conducted with a MTS 810 test machine while high strain experiments were completed with a modified split Hopkinson pressure bar. Modified SHPB had quartz crystals added to the specimen end of incident and transmitted bars and thin aluminum discs were bonded to quartz crystals to cover them from the direct impact. Experimental results indicated that failure stress increased with the increase in strain rate. Foam density was found to be effective on mechanical properties and it was observed that failure stress is directly proportional with polyurethane foam density.

Song et al [17] have studied the compressive response and failure behavior of epoxy syntactic foam. Tested material was made of epoxy resin and hollow glass microspheres where epoxy resin was used as binder and hollow glass microsphere was used as filler. Experimental part of the study was completed at low and high strain rates, having strain rate range of 10^{-4} s^{-1} to 1900 s^{-1} while a constitutive material model with

damage effects was developed through the modeling part of the study. Experimental results indicated strain rate hardening on epoxy syntactic foam at the strain rates between 550 s^{-1} and 1030 s^{-1}. Beyond these levels of strain rate, foam was softened due to strain rate induced damage. Material model used in modeling part of the study had given consistent results with the experiments.

Song et al [18] have studied the effect of strain rate on the elastic and cell wall crushing behavior of polystyrene foam. A conventional test machine was used for quasi static tests while a quartz crystal attached split Hopkinson pressure bar was occupied for the tests at high strain rates. Pulse shapers made of copper with varying thicknesses were used to reduce the slope of loading pulse. After the experiments, threshold strain value is defined for each test where strain rate became constant, thus making the test valid. It is concluded that elastic modulus and cell collapse of polystyrene foam was found to be sensitive to the changes in strain rate.

Compressive response of three different polymeric foams; namely as expanded polystyrene (EPS), high density polyethylene (HDPE) and polyurethane with two different densities on each have been investigated by Oullet et al [19]. Low strain rate testing of chosen materials were completed with an Instron conventional testing machine while a drop weight test machine was occupied for the tests at the strain rates of 10 s^{-1} and 100 s^{-1}. A polymeric Split Hopkinson Pressure Bar made of acrylic bars was used throughout the dynamic testing of polymeric foams. After the experiments, it was observed that EPS and HDPE indicated a linear region followed by increasing crush stress plateaus while linear region was followed by a plateau region with negative slope throughout the testing of polyurethane. All of the chosen polymeric foams have exhibited strain rate dependency, depicting the increase in failure stress and reduction in both failure and densification strain levels.

Song et al [20] have investigated the compressive properties of epoxidized soybean oil/clay nanocomposites. Low and high strain rate compressive tests of epoxidized soybean oil/clay nanocomposites with different percentages of nanoclay additions were conducted with a hydraulically driven test machine and a modified SHPB. Epoxidized soybean oil was mixed with clay nanocomposites with percentage of 2% and 5% while a group of specimens were intentionally left absolute to be compared through the experiments. Cylindrical cut specimens were tested with a hydraulically driven test machine at lower strain rates. A modified Split Hopkinson Pressure Bar with

the addition of quartz crystals was used through the high strain rate testing of specimens. Material model developed by Song et al (2004) was used to estimate the stress of target material. Experimental results have marked significant strain rate sensitivities and strain hardening was observed for all kinds of specimens through the experiments. One dimensional material model with five independent material constants was successful to obtain similar results with experiments.

Subhash et al [21] investigated the response of polymeric structural foams to compressive loadings at different strain rate levels. Polymeric foams used in this study had a density ranging from 0.83 $g.cm^{-3}$ to 1.46 $g.cm^{-3}$ while the porosity levels changing from 50.5% to 6.8%. Low strain rate compression tests were conducted with a servo-hydraulic test machine at the strain rate of 1.5×10^{-3} s^{-1}. A polymeric SHPB system was occupied for the dynamic testing of polymeric foams with the density lower than 1.0 $g.cm^{-3}$ while a SHPB with magnesium bars were used to compress the chosen foams with density higher than 1.0 $g.cm^{-3}$. Experiments concluded that in the quasi-static range, selected materials exhibit increased modulus of elasticity and higher ultimate stress as the bulk density increases. Also, decrease in failure strain and increase in yield stress were observed under high strain rate loading conditions.

Bryson et al [22] studied the mechanical behavior of five different polyurethane softballs under quasi-static (0.03 s^{-1}) and high strain rate (2780 s^{-1}) loading conditions. Dynamic stiffness and coefficient of restitution were the main parameters on the selection of softballs. A load frame measuring the load and displacement were used for the low strain rate tests while high strain rates were completed using a classical aluminum split Hopkinson pressure bar with dimensions of 12.7 mm in common diameter and 229 mm, 914 mm, 914 mm on striker, incident and transmitter bars, respectively. After the experiments, an increase of 20-50 percent was observed in chord modulus of polyurethane softballs due to strain rate increase. However, finite element modeling of polyurethane softballs needs extra experimental input rather than stated in this study to successfully simulate the mechanical behavior on computational environment.

Stress-strain behavior of one polyurea and three different polyurethanes with different hard segment contents were investigated by Yi et al [23]. Dynamic mechanical analysis, quasi-static compressive tests and high strain rate tests were conducted on polyurea and polyurethanes to study the mechanical behavior of chosen materials. TA

Instruments Q800 dynamic mechanical analyzer was used throughout the mechanical analyses while Instron servo hydraulic test machine and Zwick screw driven test machine were occupied for quasi-static tests and measurement of bulk modulus. A conventional aluminum split Hopkinson pressure bar was used for the dynamic compressive testing of polyurea and polyurethanes. Through the experiments, highly non-linear stress-strain behavior was observed in all of the tested polymers, depicting strong hysteresis and strong strain rate dependency. Cyclic softening was observed on some of the tested materials whereas some of polyurea and polyurethanes were found to transition from rubbery-like behavior to leathery-like behavior while one of the polyurethanes inhibited transition from rubbery-like behavior to glassy-like behavior.

Sarva et al [24] have investigated the stress strain behavior of a representative polyurea and representative polyurethane under compressive loading conditions at the strain rates ranging from 10^{-3} s^{-1} to 10000 s^{-1}. Low strain rate tests (10^{-3} s^{-1}-10^{-1} s^{-1}) were done with a Zwick screw driven mechanical tester while MTS 810 servo hydraulic test machine was used for the tests up to the strain rate of 100 s^{-1}. Two different split Hopkinson pressure bar systems with different bar lengths were used to reach the strain rates of 100 s^{-1} to 10000 s^{-1}. Intermediate strain rate SHPB, having the striker, incident and transmitter bar lengths of 3 m, 11 m and 11 m, was constructed from aluminum to reduce impedance mismatch with polymeric samples. A SHPB with 7075-T6 bars were used to deform samples beyond the strain rate of 1000 s^{-1}. After the experiments, deformation of polyurea was found to change from rubbery (10^{-3} s^{-1}) to glassy (5000 s^{-1}) whereas behavior of polyurethane shifts from rubbery to leathery with the increase in strain rate. A strong strain rate dependency is also observed through the steps of strain rate increase.

Polyurea with mass density of 1 $g.cm^{-3}$ and elastic modulus of 100 MPa was characterized by Shim et al [25]. Experiments were conducted with an Instron hydraulic universal testing machine, a classical split Hopkinson pressure bar with aluminum and nylon bars and a modified split Hopkinson pressure bar with hydraulic actuator. Instead of striker bar in conventional SHPB, modified SHPB system consisted of a hydraulic piston as the actuator and nylon bars were used as incident and transmitter bars as in classical split Hopkinson pressure bar system. Strain gages were bonded on both impact and specimen ends of incident and transmitter bars to successfully neutralize the wave dispersion in polymeric bars and transmitter bar was also fixed on non-impacted side.

Conventional split Hopkinson pressure bar systems and hydraulic test machine were occupied to validate the experimental results of modified SHPB system. Experimental results of this study confirm the known strain rate dependency of polyurea and measured stress levels correspond well with experiments conducted on conventional testing equipment. However, it was also concluded that stability of strain rate during the experiments was not possible due to finite length of input and output bars.

Muscle tissues and body parts of animals are also investigated to duplicate the impact behavior of human flesh, aiming to understand the mechanical behavior and increase the safety under dynamic loading conditions. Song et al [26] investigated compressive response of porcine muscle under various strain rates using a conventional testing machine and a modified SHPB. Since the target material is rather soft and experimental data is hard to distinguish, classical 7075-T6 aluminum SHPB was modified with the addition of semi-conductor foil strain gages on transmitted bar. Quartz crystals were added to the specimen end of both incident and transmitted bars to monitor force equilibrium at the front and back-end of specimen. Pulse shaper was also used to control the shape of loading pulse. Since the specimen is very soft and failure stress of specimen is few Megapascals, inertia effects may overshadow the material properties. To cancel out inertia effects, specimen geometry was changed from solid to annular disc. Experiments revealed that in both along and perpendicular to muscle fiber direction, strain-rate dependent behavior was observed.

Luo et al [27] have investigated Young's modulus of human tympanic membrane at high strain rates. A modified Split Hopkinson Tension Bar was used through the high strain rate experiments with the addition of an X-cut quartz crystal disk mounted on the incident bar, aiming to measure applied force. 7075-T6 aluminum incident bar and 6061-T6 aluminum hollow transmitted bar was used through the experiments. Strain rate of 2000 s^{-1} was reached through the experiments and it can be interpreted from results that Young's modulus of human tympanic membrane shows an increase with the increase in strain rate. A strong strain-rate dependency is also observed, indicating the increase of failure stress with the strain rate.

Pervin et al [28] have investigated the response of bovine liver tissue under compressive loading. Experimental determination of strain rate effect on the compressive stress-strain behavior of bovine liver tissue was aimed in this study, with the strain rates changing from 10^{-2} s^{-1} to 3000 s^{-1}. A conventional hydraulically driven

test machine was used for quasi-static and intermediate strain rates while high strain rate experiments were done with a Split Hopkinson Pressure Bar. A hollow transmission bar was used to acquire weak signals through the experiments using semi-conductor gages. Front and back face forces on the specimen were recorded via quartz crystals to ensure dynamic equilibrium. Ring-shaped specimens were tested at high strain rates to eliminate inertia effects. Experimental results show that bovine liver tissue indicates strong strain rate dependency under compressive loading, especially through the high strain rate region, regardless of the specimen direction along or perpendicular to liver surface.

Saraf et al [29] studied the dynamic response of soft human tissues using Kolsky bar technique, aiming to determine bulk modulus and shear stress of various organs in human body. Specimens were collected from heart, liver, lung and stomach of post-mortem human subjects whose causes of death did not affect the organs targeted for this study. Determination of bulk modulus was done with using an aluminum split Hopkinson pressure bar with common diameter of 12.7 mm and a confinement tube with outer diameter of 25 mm. Shear stress values of chosen materials were obtained using a shear fixture described with details in stated study. Experiments concluded that behavior of these tissues under dynamic confined compression can be represented by an approximately linear relationship between volumetric strain and pressure, indicating as the stomach being the stiffest tissue whereas the lung as the least stiff. In dynamic shearing, the behavior of these tissues is not linear elastic. Shear stress-strain curves for depicted tissues exhibit a toe region followed by a rapid growth of the shear stress with the moderate increases in shear strain.

CHAPTER 2

FUNDAMENTALS OF SPLIT HOPKINSON PRESSURE BAR TESTING OF LOW ACOUSTIC IMPEDANCE MATERIALS

2.1. Introduction

For the dynamic mechanical characterization of materials used in armor systems, SHPB testing is inevitable since the mechanical behavior changes abruptly with the strain rate. As the case investigated in this study, mechanical behavior of polymers were highly rate sensitive and previous similar studies showed the same characteristics, higher failure stresses with reduced failure strain values as the strain rate increases.

Split Hopkinson Pressure Bar, originally developed by Kolsky, is a commonly used tool to test various materials at dynamic loading conditions and also used in this thesis through the experimental study. Schematic of classical Split Hopkinson Pressure Bar setup is given in Figure 2.1.

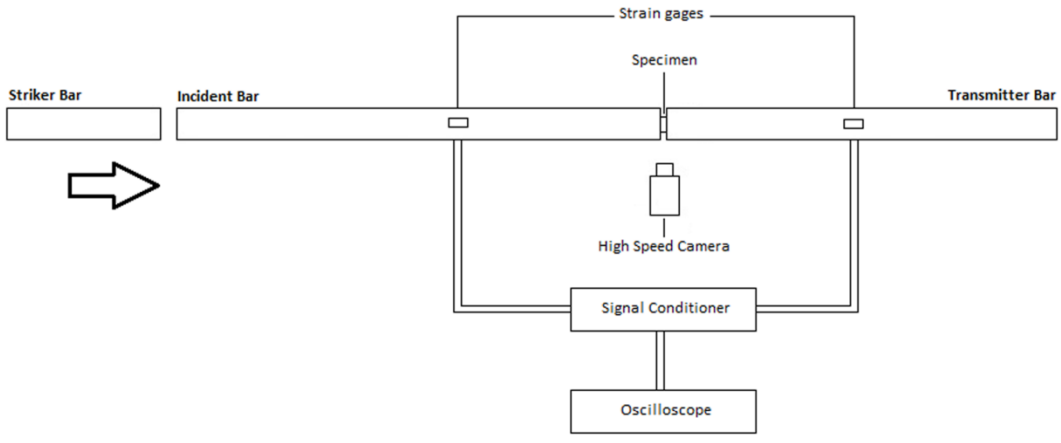

Figure 2.1. Schematic of classical Split Hopkinson Pressure Bar.

Basically, SHPB consisted of a gas gun, striker bar, incident bar, transmitted bar and the specimen sandwiched between incident and transmitted bars. In this setup, gas gun is pressurized up to a predetermined pressure. As the pressurized gas is released

from gas gun, striker bar is set into motion and an initial velocity is attained. Once the striker bar hits to the incident bar face, a stress wave is created at the impacted end of incident bar, then this wave travels down the incident bar from striker bar end to incident bar/specimen interface, called "incident wave (inc.)". When stress wave reaches the incident bar/specimen interface, part of the stress wave is transferred to specimen and caused a rapid deformation while part of stress wave is reflected back to incident bar, called "reflected wave (ref.)". As the plastic deformation occurs, stress wave travels in specimen down to transmitter bar/specimen end. At this point, part of the stress wave is again reflected in specimen while remaining part is transferred to transmitter bar, called "transmitter wave (trans.)". Loading duration of stress wave, *T*, produced in a SHPB experiment is directly proportional with the length of striker bar and defined in Equation 2.1,

$$T = \frac{2L}{C_{st}} \tag{2.1}$$

Where, L is the striker bar length and C_{st} is the elastic wave speed of the striker bar material and defined as in Equation 2.2,

$$C_{st} = \sqrt{\frac{E}{\rho}} \tag{2.2}$$

Where, E is the elasticity modulus of striker bar and ρ is the mass density of striker bar material. Velocity of striker bar is controlled with the pressure level in gas gun and magnitude of stress wave created is directly proportional with striker bar velocity. Effect of striker bar velocity on the magnitude of stress wave is given in Figure 2.2.

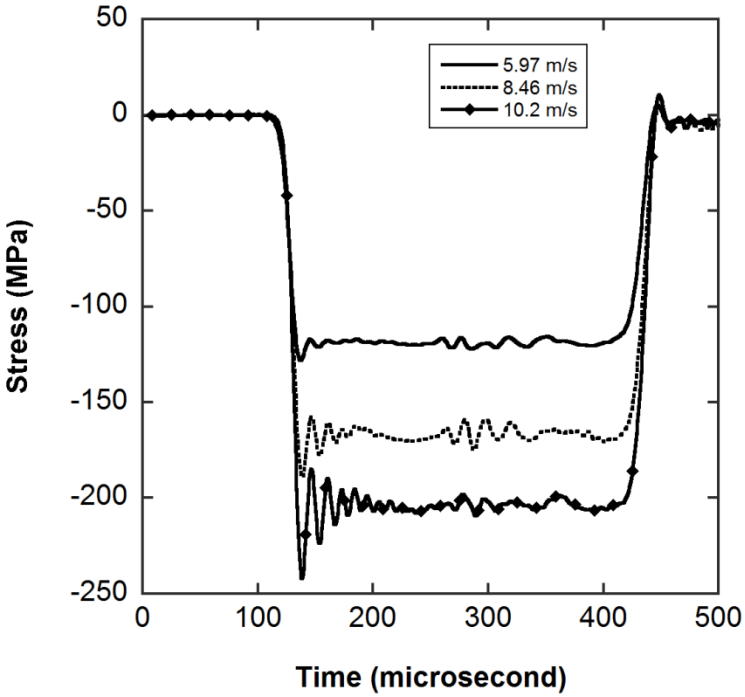

Figure 2.2. Effect of striker bar velocity on the loading pulse.

As the stress wave propagates through the bars, incident, reflected and transmitted waves are recorded with the strain gages bonded to the surfaces of bars, as given in Figure 2.1. Due to the high strength of bar materials, the applied stresses remain in the elastic deformation region, so the stress and strain values of the specimen can be measured by acquired strains as a function of time from the full bridge strain gages. Strain and stress of specimen are calculated with the following equations,

$$\varepsilon_s(t) = -2\frac{C_b}{L_s}\int_0^t \varepsilon_r dt \tag{2.3}$$

$$\sigma_s(t) = E_b\frac{A_b}{A_s}\varepsilon_t \tag{2.4}$$

Where; ε_s is the specimen strain, C_b is wave speed of bar material, L_s is the initial length of specimen, ε_r is the strain history of reflected wave, E_b is the Young's modulus of bar material, ε_t is the strain history of transmitter bar, A_b and A_s are the bar and specimen areas, respectively.

Equations given above are only valid if there is force equilibrium in front and back faces of specimen. State of force equilibrium is checked with dimensionless R parameter defined in Equation 2.5,

$$R = 2\frac{(F_1 - F_2)}{(F_1 + F_2)} \tag{2.5}$$

Where F_1 and F_2 are defined as front and back forces measured on the specimen. Extent of deviation of stress is defined by R parameter and when the R reaches 0, stress equilibrium is reached in specimen.

2.2. Objective and Method

Previous studies showed that low acoustic impedance materials used in armor systems successfully reduced the transmitted stress values and caused significant amount of time delay. For a typical ballistic impact event, when the projectile hits the target, layers of armor are compressed as the course of penetration. In order to have better ballistic protection, this intrinsic low acoustic impedance characteristic must be kept at higher strain levels. In this study, two different low acoustic impedance materials, Teflon and Polyurethane, were mechanically characterized at both quasi-static and high strain rates and the potential applicability of both materials as interlayer material in multilayered armor systems was investigated.

Quasi-static tests serve to understand the behavior of materials at low strain rates whereas Split Hopkinson Pressure Bar experiments represent dynamic loading conditions as well as propagation of stress wave in a single layered material. As described above, during an SHPB experiment, specimen is deformed with rapid compression of incident bar due to compressive stress wave created with the impact of striker to incident bar. Due to theory of dynamic testing with SHPB, bars are considered to remain on elastic region. In order to satisfy this condition, metals with high yield strength is generally used as bar material and this result in a difference in terms of density and acoustic impedance during the testing of soft materials. As the one dimensional stress wave propagates in bar and specimen on Z-axis only, both materials

can be defined as medium with own characteristics hence term of acoustic impedance is defined in Equation 2.6 as,

$$Z_0 = \rho c \tag{2.6}$$

where Z_0, ρ and c are defined as acoustic impedance, density of medium and wave speed, respectively. Using Equations 2.2 and 2.6, ratio of acoustic impedances of Teflon and CPM Rex 76 steel were calculated as 490.78. As expected, preliminary SHPB tests of Teflon with CPM Rex 76 bars were found to be problematic since it is hard to distinguish experimental data from the electrical noise in transmitter bar signals. After the preliminary testing of Teflon, it was thought to be necessary to change or modify the classical Split Hopkinson Pressure Bar. For this purpose, there are three different routes available to overcome this problem: i) changing bar material with polymers such as acrylic to reduce impedance mismatch, ii) using hollow transmitter bar to reduce density and wave speed to reduce acoustic impedance of transmitter bar and iii) modifying the classical split Hopkinson pressure bar by adding piezoelectric transducers to directly measure the force at the specimen/bar interfaces.

Previously, Zhao et al [30] investigated usage of low impedance polymeric bars to reduce impedance mismatch. When polymeric bars are used, a sufficiently large diameter of both specimen and bar is necessary for two reasons: small diameter specimen may not represent the behavior of material and dynamic buckling may occur in polymeric bars with small diameter during the test. However, dispersion correction must be applied to neutralize wave dispersion effects in bars and striker length must be reduced to eliminate time extension of the incident wave. Wang et al [31] also focused on using polymeric bars and generalization of Split Hopkinson Pressure Bar technique to use viscoelastic bars. Based on Zhu-Wang-Tang viscoelastic constitutive equations [31], authors of the study developed an experimentally confirmed generalized method for usage of polymeric bars. However, dispersion and dissipation behavior of wave propagation in polymeric bars must be taken into account to avoid erroneous results.

An alternative method for testing soft materials was proposed by Chen et al [32] to overcome the problems encountered using viscoelastic bars. 7075-T651 high strength aluminum was used as bar material in striker and incident bars while hollow transmitter bar was used to reduce acoustic impedance mismatch between soft specimens and

transmitter bar. After the experiments conducted with RTV 630 silicon, it was concluded that using hollow bar enabled the termination of physical effects of viscoelastic bars. However, this method had just improved the amplitude of transmitter wave by an order of magnitude but did not affect the amplitude of noise. Furthermore, if chosen material to be tested has very low strength and acoustic impedance, more reliable experimental technique with higher sensitivity in transmitter bar signal must be developed to characterize such materials at high strain rates.

In addition to methods of polymeric and hollow bar usage, insertion of quartz crystals either to the middle of transmitter bar [15] or specimen ends of both incident and transmitter bars [16-18, 20, 26, 28] were offered to characterize soft materials. Quartz crystals with acoustic impedance very close to bar material are used in modified SHPB setups. Thin disks of bar material were also used to protect brittle crystals from direct impact. Quartz crystals allow direct measurement of force at both ends of specimen and more accurate noise-free data can be recorded during SHPB experiment. Moreover, force equilibrium in a SHPB experiment can be verified with the data acquired from quartz crystals.

When the aforementioned solution methods are considered, the quartz crystal implementation to SHPB setup was selected in the current study. Two differently behaving materials, one with low Poisson's ratio and the other with high, were characterized in this study.

The first material characterized is Teflon. Due to its low strength and acoustic impedance, the strain read-outs from the strain-gage on the transmitter bar surface are low even at comparable levels with the electrical noise occurring in the signals. Thus, quartz crystals are used at the specimen/transmitter bar interface in order to directly measure the force values during SHPB tests. 7075-T6 Aluminum bars were also used and the acoustic impedance mismatch between bar and specimen was lowered. Details of quartz crystal insertion to transmitter bar end are given in Chapter 3.

The second material characterized is Polyurethane. Preliminary SHPB testing on Polyurethane showed that the transmitted bar signals are significantly higher than those of Teflon. Thus, signals could successfully be captured using the regular strain gages on the bar surfaces. However, main problems encountered with Polyurethane are oscillations in transmitted bar signals. In order to overcome this, pulse shaping was applied. In this method, the loading rate, slope of compressive pulse, is modified by

placing soft materials between striker and incident bars end, called “pulse shapers” [15-18, 20, 24, 26, 28]. In this study, rectangular prisms of EPDM rubber were deformed to change the shape of stress wave propagating in incident bar. Details of pulse shaping are given in Chapter 3.

Mechanical characterization involves quasi-static and high strain rate experiments. During Split Hopkinson Pressure Bar tests, real time deformation of samples was recorded with a high speed camera at 10800 fps and 22500 fps.

Outputs of experimental study, both experimental data and high speed camera recordings, were the main sources of input for the numerical study. Strain gage read-outs in a typical experiment include voltage history, allowing the measurement of strain and stress of specimen as well as those of bars, impact velocity of striker bar and average strain rate. Finite element model of SHPB uses some of the experimental data such as stress-strain curve as input and if well-defined, numerical model of split Hopkinson pressure bar can successfully predict additional parameters such as stress and displacement of each node, internal energies and force levels on bar interfaces, all of which can be acquired as function of time. Details of numerical study are given in Chapter 4.

CHAPTER 3

MATERIALS AND EXPERIMENTS

3.1. Introduction

Characterization of Teflon and Polyurethane were done with experiments conducted at various strain rates. Experimental study has begun with preparation of specimen from both materials. Specimens then were compression tested at both quasi-static and high strain rates using Shimadzu AG-I conventional test machine and Split Hopkinson Pressure Bar, respectively.

3.2. Materials

3.2.1. Gore™ Polarchip™ Heat Insulating Teflon

The first material to be characterized was Gore™ Polarchip™ heat insulating Teflon. This material consisted of expanded polytetraflouroethylene (ePTFE) and boron nitride (BN) is ideal for the applications of filling gaps where large or variable gaps occur due to irregular surfaces. Ability of good formability and softness was gained with matrix material ePTFE while additions of BN particles increase thermal conductivity.

In this study, Teflon was received in sheet form from the manufacturer. Cylindrical Teflon specimens were cut with a core-drill, having a common thickness of 2.00 mm and diameter ranging from 12.00 mm to 17.40 mm. A Teflon specimen core – drilled with a bench type drill before an experiment is given in Figure 3.1.

Figure 3.1. Core-drilled Teflon specimen before experiment.

3.2.2. Dow Chemicals™ Voracor CS Polyurethane

The second material investigated in this study was Dow Chemicals™ Voracor CS Polyurethane. Originally developed for thermal insulation in buildings, this material can also be sprayed on various surfaces for water isolation. Voracor CS Polyurethane consists of Voracor CS 1344 Polyol and Voracor CS 1293 Isocynate while the polyol also consist of HCFC 141b blowing agent to make the form of polymeric foam. During the application on a surface, components of Polyurethane are mixed and sprayed on target surfaces using high pressure pumps.

In this study, Polyurethane was received in sheets with varying thicknesses. At the first stage of specimen preparation, Polyurethane was surface grinded to insure parallel faces. Surface grinded Polyurethane sheet was then core drilled with a bench type drill and cylindrical specimens were obtained with dimensions of 2.80 mm in

thickness and 14.50 mm in diameter. Polyurethane sheet, core-drill and specimen before test are given in Figure 3.2.

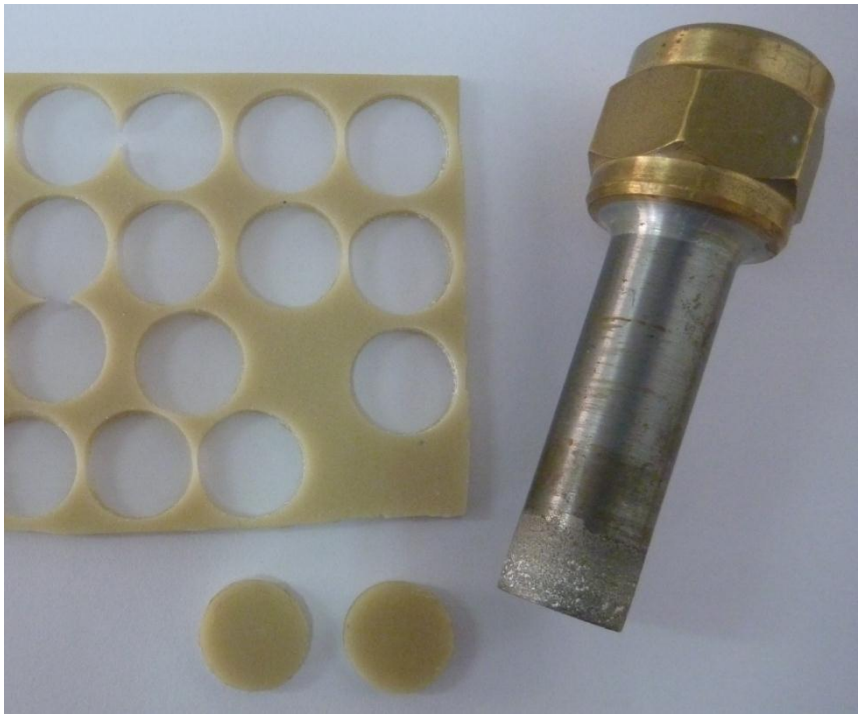

Figure 3.2. Core-drilled Polyurethane specimen before experiment.

3.3. Experiments

3.3.1. Quasi-Static Tests

Quasi-static tests were done at the Dynamic Testing and Modeling Laboratory, IZTECH with both Teflon and Polyurethane to obtain material data under quasi – static loading conditions. Shimadzu AG-X conventional mechanically driven testing machine with the capacity of 300 kN was used through the experiments, as given in Figure 3.3.

Figure 3.3. Shimadzu AG-X test machine used through the quasi-static tests.

Strain rate was controlled with the cross head speed. As the cross head speed increases, strain rate increases and specimen is deformed rapidly. Desired cross head speed can be determined with the desired strain rate with Equation 3.1,

$$v_{cr} = \dot{\varepsilon} \times L \tag{3.1}$$

Where v_{cr} represents cross head speed, $\dot{\varepsilon}$ represents strain rate and L represents length of specimen. Stress – strain curves of polyurethane and Teflon were obtained at the strain rates of 10^{-3}, 10^{-2} and 10^{-1}.

3.3.2. High Strain Rate Tests

High strain rate tests were carried out using two different Split Hopkinson Pressure Bar setups. In addition to quasi-static tests, characterization of Teflon and Polyurethane was done with implementation of quartz crystals to incident bar and pulse shaper usage during SHPB testing to overcome the problems encountered on testing of materials with low acoustic impedance.

Initial testing done on Teflon presented a significant amount of noise in the signals acquired from the strain gages due to impedance mismatch between specimen and bar material, given in Figure 3.4. Transmitted bar stress levels are remained low as compared to those of incident. 7075-T6 aluminum bars were used for this purpose during the study and also classical Split Hopkinson Pressure Bar was modified with insertion of quartz crystals.

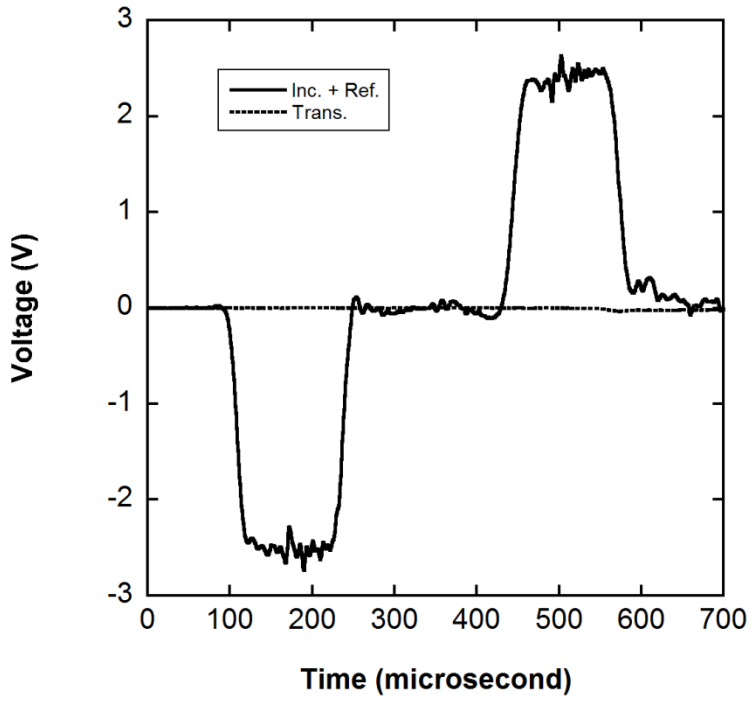

Figure 3.4. Experimental data of Teflon recorded with Steel SHPB.

The specimen strain was calculated from the reflected wave, the voltage level of which remained high during the test. Since the voltage level from the transmitter bar was significantly lower than that of incident, a quartz crystal was added to the specimen/transmitter bar end to allow direct force measurement and improve accuracy

of stress measurement. In this study, Boston Piezo-Optics X-cut quartz crystals with thickness of 0.254 ± 0.01 mm in same diameter with bars and had a mechanical impedance very similar to that of bar material (bar: 14.19 x 10^6 $kg.m^{-1}.s^{-2}$ quartz crystal: 15.11 x 10^6 $kg.m^{-1}.s^{-2}$ ratio: 1.06) were used. An example of quartz crystal before bonding is given in Figure 3.5.

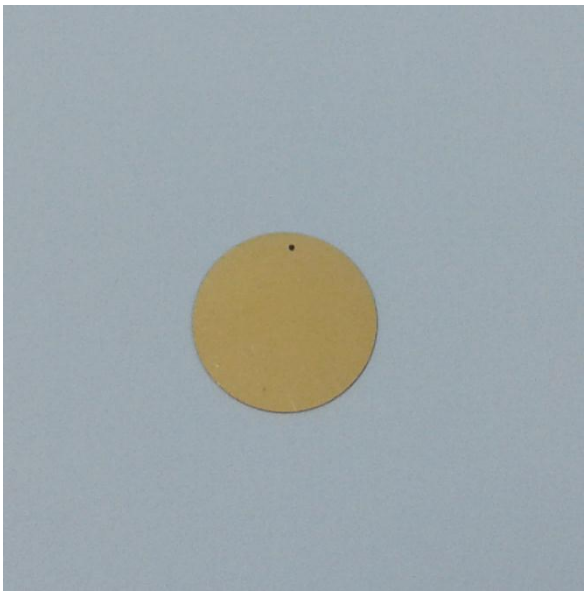

Figure 3.5. Quartz crystal before bonding.

During the insertion of quartz crystals; specimen and bar ends were cleaned and degreased. Then equal amounts of epoxy and hardener of CircuitWorks CW 2400 conductive epoxy were taken and mixed about 3 minutes. Mixture of epoxy and hardener was smeared on specimen end of transmitter bar and quartz crystal to start bonding. Marked with a dot, positive pole of quartz crystal was faced to specimen and covered with a 3 mm thick aluminum platen bonded by conductive epoxy to prevent damaging during the experiment. Solidification of epoxy was further accelerated and curing was completed with local heating of cohesion area. When the solidification was finished, poles of quartz crystals were checked with a multimeter and excessive conductive epoxy was cleaned off to avoid short circuiting. Both platen and transmitter bar were drilled about 3 mm for quartz crystal cabling and quartz crystal was connected to Kistler 5010A charge amplifier. Charge created in quartz crystal due to the applied loading can be measured in terms of voltage with a piezoelectric constant of $-2.3x10^{-12}$ $C.N^{-1}$, output of charge amplifier to LDS Genesis data acquisition system was quartz

crystal voltage as a function of time since measured force was converted into voltage with constant of 2000 $N.V^{-1}$. Real time deformation of Teflon during SHPB experiments were also recorded with Photron FastCam high speed camera. Schematic of modified SHPB set-up for dynamic testing of Teflon is given in Figure 3.6.

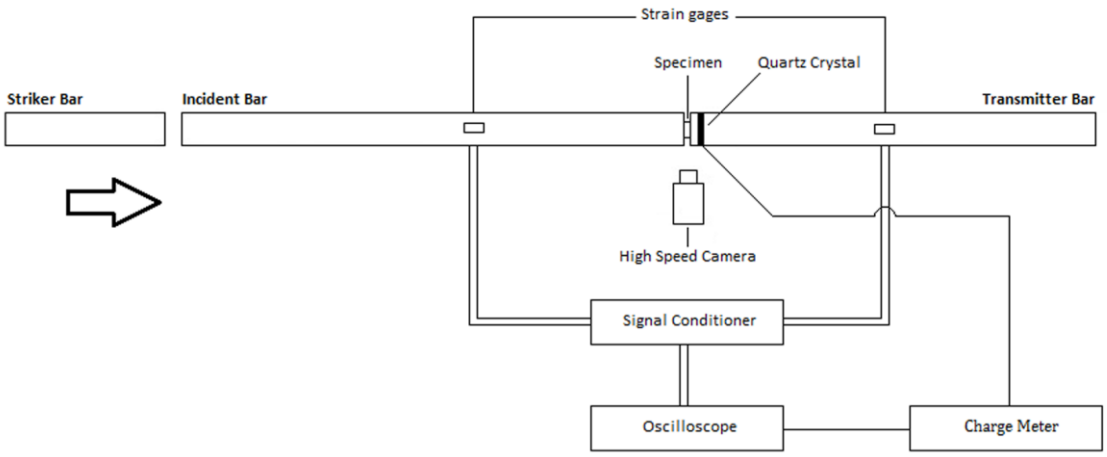

Figure 3.6. Schematic of modified SHPB used in dynamic testing of Teflon.

During the SHPB tests of Polyurethane pulse shaper were used to change the slope and shape of loading pulse by placing an easily deforming material between striker and incident bars. Schematic of a pulse shaper implemented SHPB setup is given in Figure 3.7.

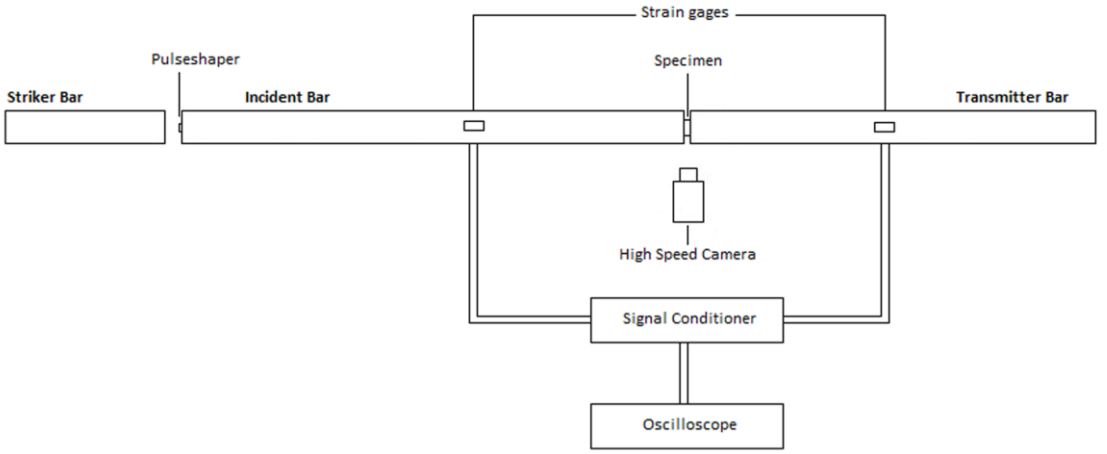

Figure 3.7. Schematic of pulse shaper implemented SHPB.

In this study, EPDM rubber was used as pulse shaper. As received EPDM rubber was in sheet form with the dimensions of 1200 mm, 300 mm, 3 mm in length,

width and thickness, respectively. Final form of the pulse shaper has the dimensions of 1.5 mm, 1.5 mm, 2 mm in length, width and thickness, respectively. Dimensions of pulse shaper were changed according to velocity of striker bar. A pulse shaper ready for experiment is given in Figure 3.8.

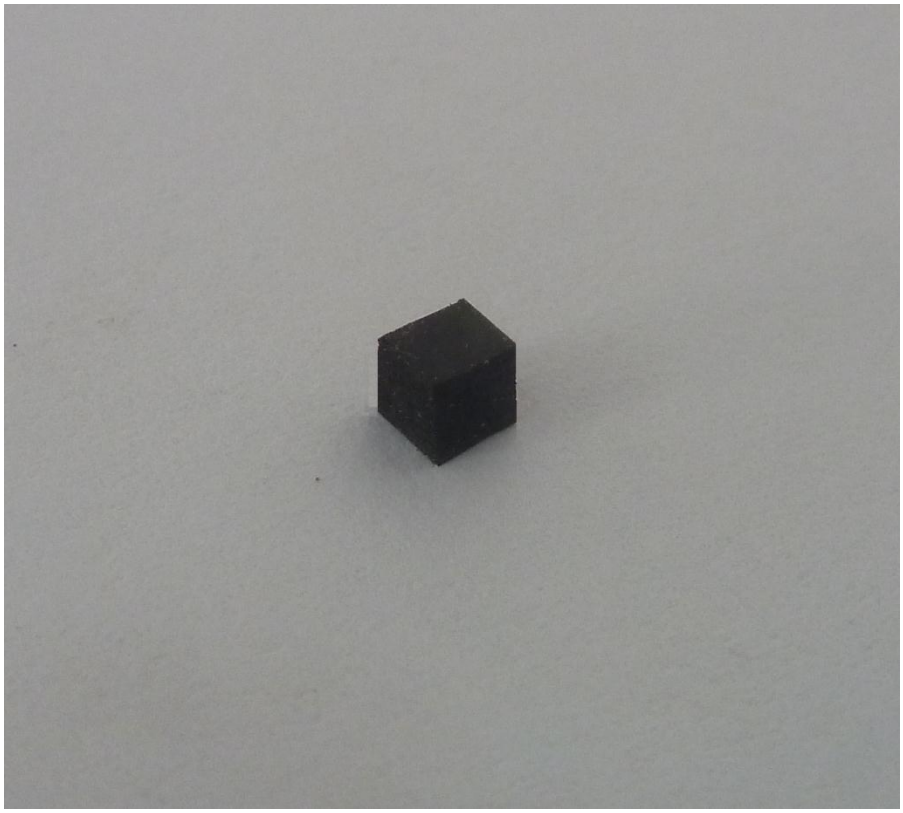

Figure 3.8. Pulse shaper ready for experiment.

The effect of pulse shaper on the loading pulse can be seen in Figure 3.9. A regular loading pulse in Split Hopkinson Pressure Bar is in trapezoidal shape with a steep slope, while this shape of loading pulse is converted to concave upwards profile with a relatively lower slope when pulse shaper is used, enabling a smoother loading of specimen.

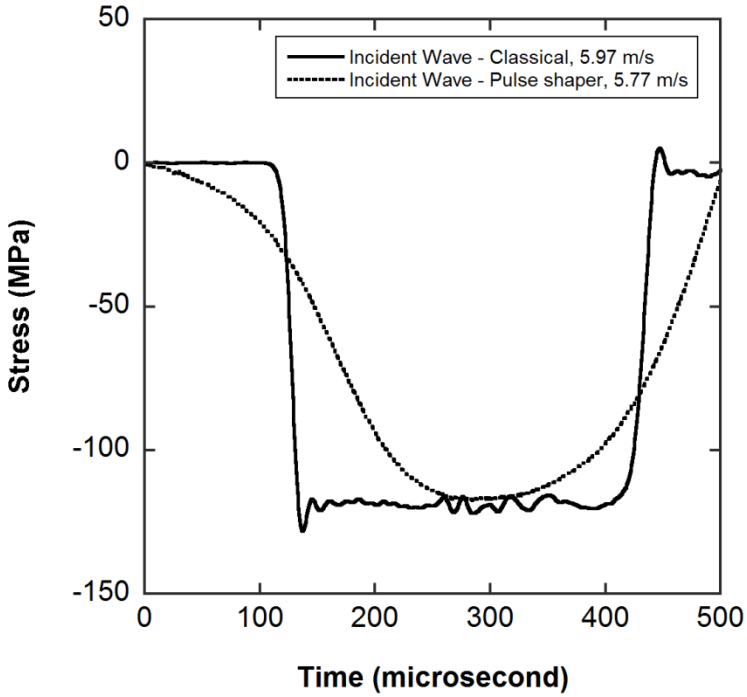

Figure 3.9. Comparison of a standard compression wave and pulse shaper used compression wave.

CHAPTER 4

FINITE ELEMENT MODELING

4.1. Model Description

Split Hopkinson Pressure Bar tests were modeled to study the stress wave propagation and dynamic deformation of the materials. Commercially available finite element software LS-DYNA was used through the numerical studies. Meshes of Split Hopkinson Pressure Bar and specimens were generated using LS-INGRID. Fully symmetric numerical model of SHPB was prepared using eight-node solid elements. Experimental and numerical bar responses are compared and close agreement of results are checked to verify the finite element model. As discussed in Chapter 2, velocity of striker bar and strains of bars as a function of time can be measured with strain gages in an actual SHPB experiment. When verified with good correlation of bar responses to experiment, finite element model of SHPB can give the output of displacement of nodes, strains and stresses of elements, force levels on bar interfaces, global and material energies as well.

Finite element model of Split Hopkinson Pressure Bar contained three components in contact; specimen, incident and transmitter bars. All of the components were modeled with the dimensions of experimental set-up. In this study, input pulse propagating through the incident bar was determined in two methods; either defining an experimentally determined pressure pulse onto the incident bar face or explicitly modeling striker bar and assigning an initial velocity to it. Former method was used in modeling of Teflon and latter for Polyurethane since pulse shaping was used. Mesh biasing is applied in modeling of both Teflon and Polyurethane to refine the meshes in interfaces of contact. Mesh sensitivity study was conducted in order to determine the optimum mesh size. For this purpose, three different mesh sizes were used, average element size of which was 0.225 mm and the optimum mesh size was determined as 0.2 mm for both Teflon and Polyurethane. Specimens of Teflon and Polyurethane are given in Figure 4.1 and Figure 4.2, respectively.

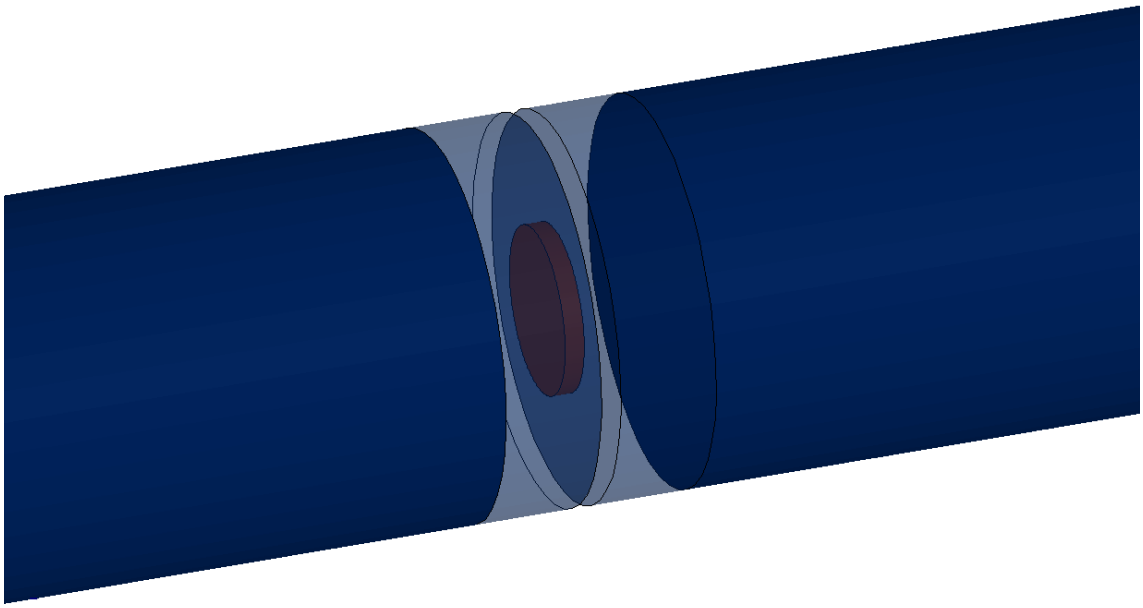

Figure 4.1. Finite element model of Teflon.

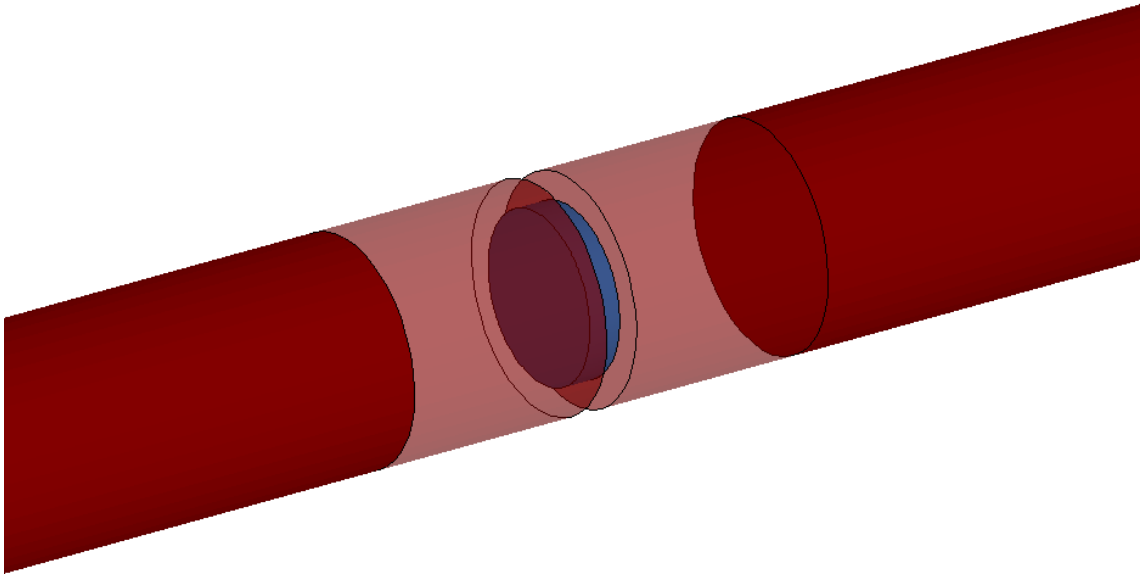

Figure 4.2. Finite element model of Polyurethane.

The material model 63, *MAT_CRUSHABLE_FOAM, was used during the numerical modeling of Polyurethane and Teflon. This material model was developed to represent the behavior of strain rate sensitive crushable foams with optional parameters such as damping coefficient and tension cut-off stress. Through the implementation, stress in elements was updated using the Equation 4.1,

$$\sigma_{ij}^{trial} = \sigma_{ij}^{n} + E\dot{\varepsilon}_{ij}^{n+1/2}\Delta t^{n+1/2} \quad (4.1)$$

Where σ_{ij} is principal stresses, E is modulus of elasticity, $\dot{\varepsilon}_{ij}$ is principal strain rate and Δt is time interval of solution. Magnitude of principal stresses (i=1, 3) are checked if the value of yield stress is exceeded and if so, they are scaled back to the yield surface using Equation 4.2,

$$if\ \sigma_y < \left|\sigma_i^{trial}\right|, \sigma_i^{n+1} = \sigma_y \frac{\sigma_i^{trial}}{\left|\sigma_i^{trial}\right|} \quad (4.2)$$

For a valid Split Hopkinson pressure bar test, incident and transmitter bars must remain elastic, thus bar material was modeled using material model 1, *MAT_ELASTIC. This material model was developed for isotropic elastic behavior for beam, shell and solid elements in LS-DYNA. Contact between specimen and bars were modeled using CONTACT_ERODING_SURFACE_TO_SURFACE card with specimen chosen as 'slave' while static and dynamic coefficient of friction was selected as 0.3 and 0.2, respectively. Time step calculation was done with automatic time step calculation option was used with CONTROL_TIMESTEP. In this option, LS-DYNA determines step size by looping through the elements and taking the minimum value over all elements. Determination of time step is given in Equation (4.3),

$$\Delta t^{n+1} = TSSFAC \times \min(\Delta t_1, \Delta t_2, \dots, \Delta t_N) \quad (4.3)$$

Where, TSSFAC and N are scale factor for computed time step and total number of elements, respectively. Time step size roughly corresponds to transition time of a wave through an element using the shortest characteristic distance. Default value of 0.90 was determined by LS-DYNA and was sufficient enough to duplicate wave characteristics. Material properties of Teflon, Polyurethane and bar materials are given in Table 4.1 and 4.2.

Table 4.1. Material properties of Teflon and Polyurethane used in numerical study.

Material	**Modulus of Elasticity (GPa)**	**Poisson's Ratio**	**Density ($kg.m^{-3}$)**	**Other**
Teflon	9.65×10^{-3}	0.01	760	TSC = 50 MPa DAMP = 0.05
Polyurethane	0.2	0.25	1200	TSC = 50 MPa DAMP = 0.3

Table 4.2. Material properties of bar materials used in numerical study.

Material	**Modulus of Elasticity (GPa)**	**Poisson's Ratio**	**Density ($kg.m^{-3}$)**
Vascomax™ C-350 Maraging Steel	200	0.267	8080
7075-T6 Aluminum	71.7	0.33	2810

CHAPTER 5

RESULTS

5.1. Results of Experimental Study

5.1.1. Quasi – Static Test Results

Polyurethane and Teflon were tested at strain rates of 10^{-3} s^{-1}, 10^{-2} s^{-1} and 10^{-1} s^{-1} using Shimadzu AG-X universal test machine under compression. Before the experiments, average strain rate of each test was calculated using Equation 3.1. During the tests, force and cross-head displacement data were recorded. Video extensometer was also used to measure the specimen strain. This data is then converted to stress-strain graphs at each strain rate.

Quasi-static test results of Teflon are given in Figure 5.1. It can be seen from figure that all of the tests in quasi-static range showed similar characteristics under quasi-static compressive loadings regardless of strain rate. All three curves started with a linear region, a plateau region with a slight slope then this region was followed by densification. Densification strain was found to vary with strain rate. At the average strain rate of 10^{-3} s^{-1}, a maximum stress of 15 MPa was reached at a strain of 0.85 while maximum strain was reduced to 0.77 for the average strain rate of 10^{-2} s^{-1}. Maximum strain was further reduced to 0.6 at the average strain rate of 10^{-1} s^{-1}. Macroscopically, Teflon was found to fail completely after the experiments and tested specimens were smeared on both ends of cross-heads.

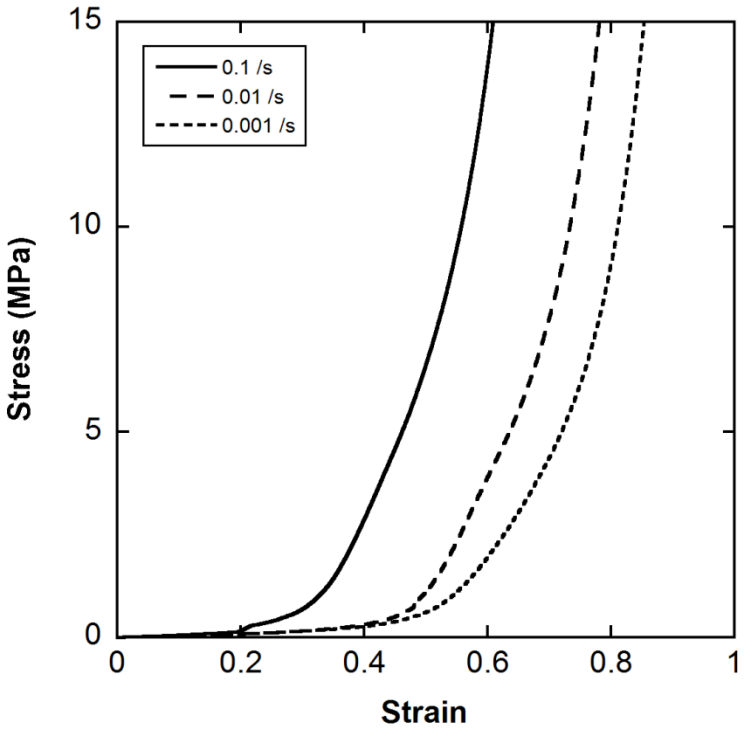

Figure 5.1. Quasi-static test results of Teflon.

Polyurethane was tested at average strain rates of 10^{-3} s^{-1}, 10^{-2} s^{-1} and 10^{-1} s^{-1} and results are given in Figure 5.2. It can be interpreted from the figure that Polyurethane shows a linear region up to a strain of 0.1 in all of the quasi-static tests conducted. Above the strain of 0.1, a plateau region with a slight slope was observed regardless of strain rate. As strain is increased, a sudden increase in stress of Polyurethane was observed in quasi-static tests, showing the initiation of densification. At the average strain rate of 10^{-3} s^{-1}, maximum stress of 85 MPa was reached at the strain of 0.8 while maximum stress was increased to 95 MPa at the average strain rate of 10^{-2} s^{-1}. As the average strain rate was increased to 10^{-1} s^{-1}, maximum stress reached on polyurethane was increased to 100 MPa while peak strain value was reduced to 0.76. On macroscopic scale, when force was removed, instantaneous elastic recovery was observed with no significant damage.

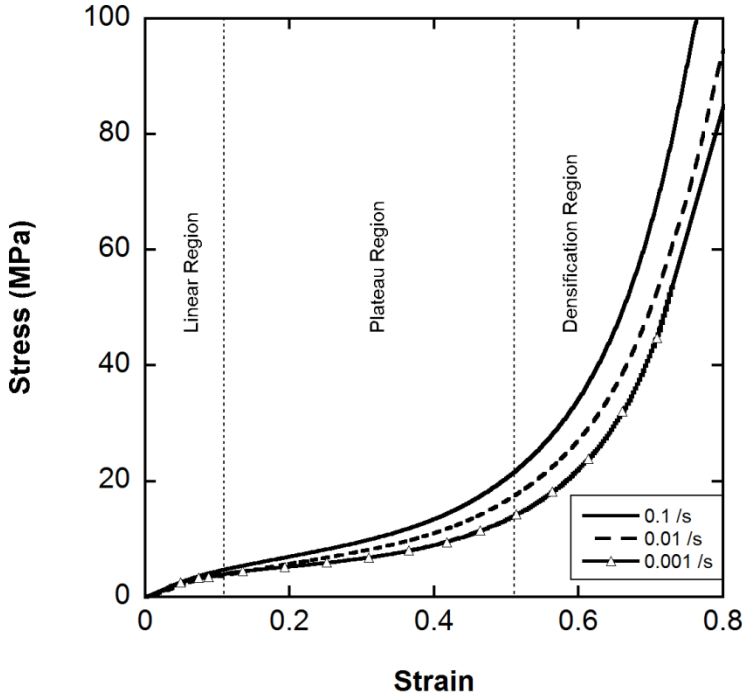

Figure 5.2. Quasi-static test results of Polyurethane.

5.1.2. Dynamic Test Results

Dynamic testing of Teflon was carried out using 7075-T6 aluminum Split Hopkinson Pressure Bar with quartz crystal implemented. Typical data recorded through a SHPB experiment of Teflon is given in Figure 5.3. Solid and dashed lines in Figure 5.3 represent the signals measured with strain gages mounted on incident and transmitter bars, respectively while dotted line represents the recordings of quartz crystal. During the experiment, initial rise of compressive pulse in transmitter bar was observed about 275 μs in quartz crystal recordings while strain gage on transmitter bar has started to obtain signals at 380 μs. The difference between initiation of data acquisition in quartz crystal and strain gage can be related with the position of those sensors on transmitter bar. Also, a good correlation was observed in transmitter bar signals acquired with strain gage and quartz crystal in terms of amplitude and magnitude of signal.

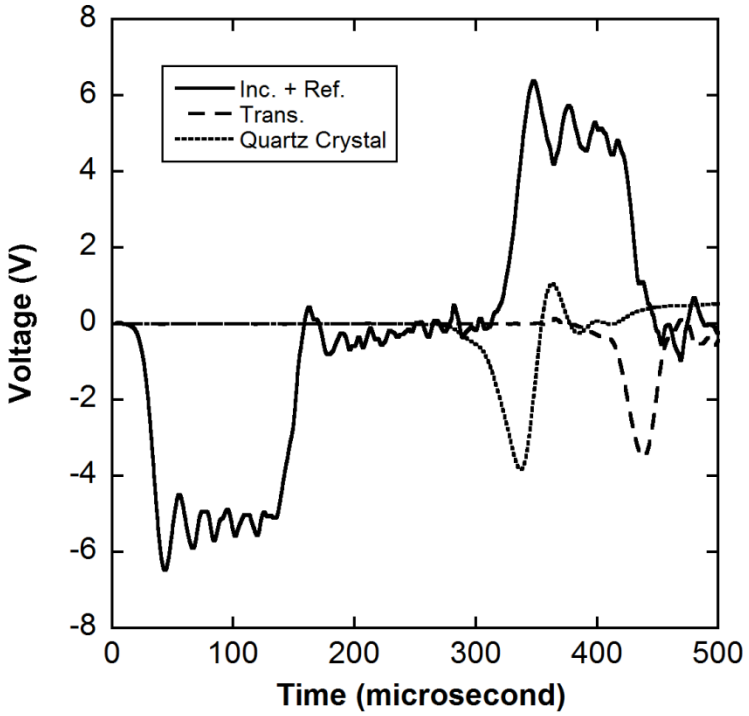

Figure 5.3. Experimental data recorded from modified SHPB.

As stated in Chapter 2, strain and strain rate of a SHPB test can be altered by varying the striker bar velocity. During SHPB testing of Teflon, striker velocity of 16.34 m/s and 21.42 m/s were reached, resulting the average strain rates of 7200 s^{-1} and 9500 s^{-1} in experiments, respectively. High strain rate test results of Teflon at the average strain rates of 7200 s^{-1} and 9500 s^{-1} were given in Figures 5.4 and 5.5, respectively. It can be interpreted from aforementioned figures that measurements of stress with strain gages involved oscillations up to strain of 0.08 and followed by underestimation of specimen stress up to the strain of 0.15. Above the strain of 0.15, stress-strain curves of strain gage and quartz crystal tend to follow similar trend. Both of quartz crystal and strain gage have reached the same level of maximum strain and maximum stress during SHPB testing. At the average strain rate of 7200 s^{-1}, a maximum stress around 10 MPa was reached at a strain of 0.3 while maximum stress was increased to 80 MPa at the average strain rate of 9500 s^{-1}. After SHPB tests, Teflon specimens were failed completely and smeared to impact end of transmitter bar.

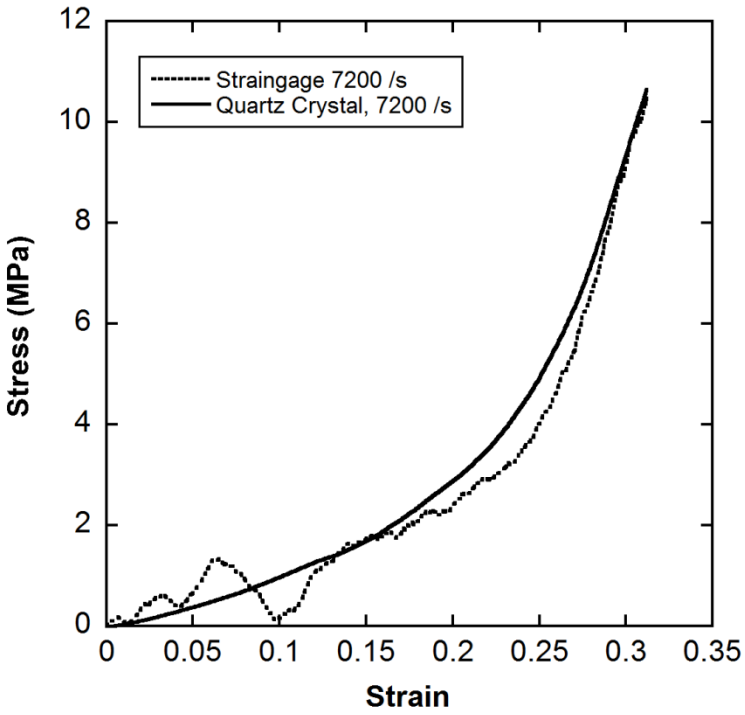

Figure 5.4. Stress-strain graph of Teflon at the average strain rate of 7200 s^{-1}.

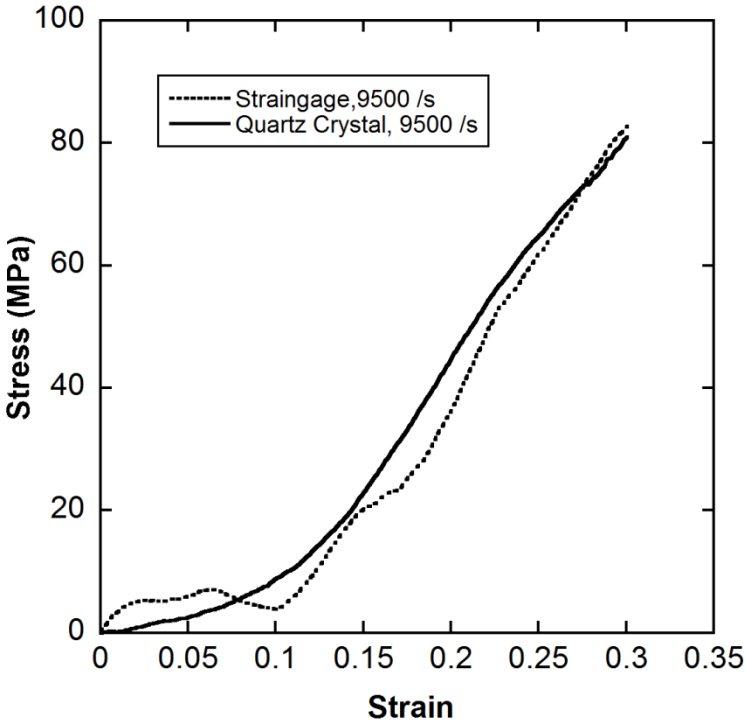

Figure 5.5. Stress-strain graph of Teflon at the average strain rate of 9500 s^{-1}.

High strain rate testing of Polyurethane was carried out using steel Split Hopkinson Pressure Bar. Bar material was selected as VASCOMAX C350 maraging steel due to material's superior mechanical properties and typical experimental data recorded during the testing of Polyurethane is given in Figure 5.6. It can also be seen from figure that oscillations in the loading and output pulses were reduced by the deformation of EPDM rubber pulse shaper between striker and incident bars. Dimensions of pulse shaper were determined by conducting empty tests (no specimen between the bars) for various striker bar velocities. When a striker of 700 mm was used, pulse shaper of EPDM cube with a side dimension of 1.5 mm was used for the SHPB testing of Polyurethane at lower strain rates. For the tests at higher strain rates, the shape of pulse shaper was changed to rectangular prism accordingly to dimensions of 1.5 mm x 1.5 mm x 2 mm.

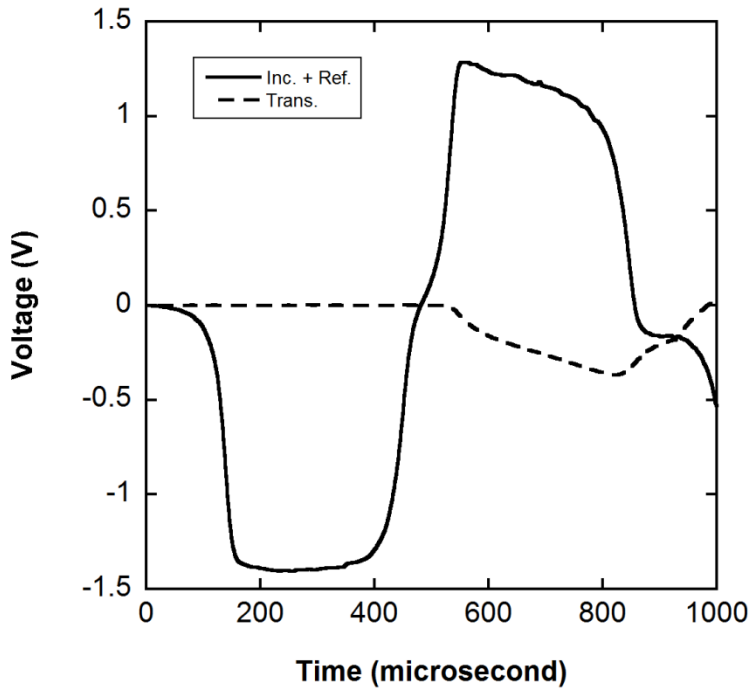

Figure 5.6. Experimental data recorded during the dynamic testing of Polyurethane.

Dynamic compression stress-strain curves of Polyurethane are given in Figure 5.7. Triangle-marked line in Figure 5.7 represents the lowest strain rate achieved through the SHPB testing of Polyurethane (1360 s^{-1}) whereas dashed line and solid line represent the two other results of SHPB tests at the average strain rates of 1650 s^{-1} and 2260 s^{-1}, respectively. Results indicate that regardless of strain rate, stress-strain

behavior of Polyurethane follow a similar trend of curves with two different slopes on each. Up to a strain of 0.1, all of the curves represent a linear region with steeper slopes when compared to quasi-static tests. As the strain of 0.1 was reached, slope of strain-stress curve was reduced, again regardless of strain rate. At the average strain rate of 1360 s^{-1}, maximum stress of 42 MPa was reached at a strain of 0.35 while maximum stress was increased to 56 MPa and 107 MPa at the average strain rates of 1650 s^{-1} and 2260 s^{-1}, respectively. All three curves indicated unloading after reaching maximum stress values at the average strain rates. On macroscopic scale, no visible damage or rupture was also observed on specimens subjected to dynamic compressive loadings.

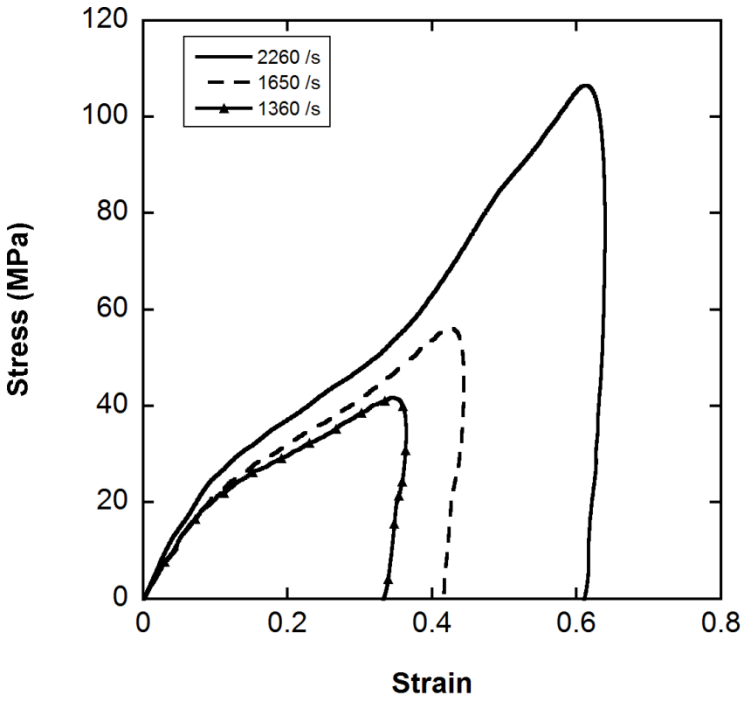

Figure 5.7. Stress-strain graph of Polyurethane at high strain rates.

5.2. Results of Numerical Study

SHPB experiments conducted with Teflon and Polyurethane were numerically modeled using LS-DYNA finite element software. Bar response of an SHPB experiment done with Teflon was compared with numerical study in Figure 5.8. In this figure, dotted line represents the SHPB experiment of Teflon while solid line represents the result of numerical study and both curves were shifted in time domain to simplify distinguishing. As seen from Figure 5.8 that numerical study agreed well with

experiment in terms of amplitude and magnitude of stress waves both in incident and transmitter bars. It was also concluded that the wave propagation in aluminum SHPB was well duplicated with numerical model of Teflon and allowed to have detailed information about “black box” of SHPB testing with additional outputs mentioned in Chapter 6.

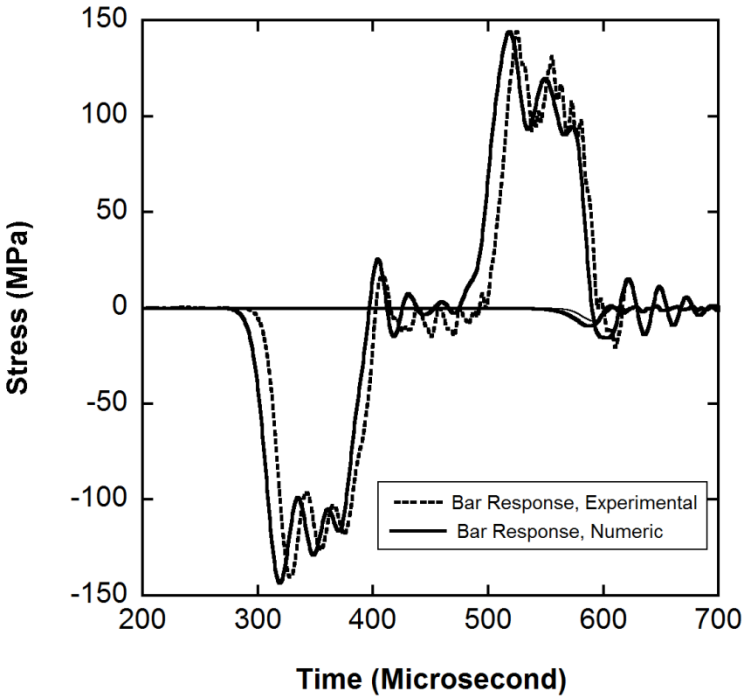

Figure 5.8. Comparison of experimental and numerical bar responses of Teflon.

Numerical bar response of Polyurethane was compared with an SHPB experiment in Figure 5.9. Bar response of numerical study on Polyurethane is represented with dotted line while bar response of experiment conducted with steel SHPB is represented with solid line. Both of the curves again intentionally shifted in time domain to simplify distinguishing the results of numerical and experimental studies. A good correlation was observed between numerical and experimental study in shape of bar responses both in incident and transmitter bars. Matching of bar responses also concluded that wave propagation in steel SHPB was well modeled through the numerical study and allowed having further information on SHPB testing of Polyurethane, mentioned in Chapter 6.

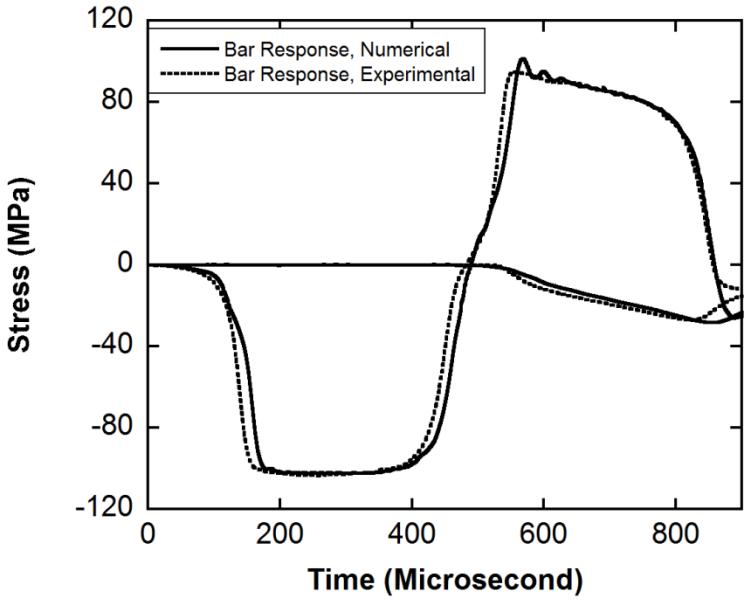

Figure 5.9. Comparison of experimental and numerical bar responses of Polyurethane.

CHAPTER 6

DISCUSSIONS

As stated in previous chapters, experimental study involves testing of Teflon and Polyurethane at various strain rates. Mechanical properties of both materials were determined with quasi-static and high strain rate compression tests, reaching the lowest strain rate of 10^{-3} s^{-1} in quasi-static tests while 2260 s^{-1} and 9500 s^{-1} in SHPB tests of Polyurethane and Teflon, respectively.

Through the experimental study, quasi-static tests of Teflon were conducted at the strain rates of 10^{-3} s^{-1}, 10^{-2} s^{-1} and 10^{-1} s^{-1} while strain rate was increased to 7200 s^{-1} and 9500 s^{-1} during SHPB tests. Compression stress strain curves of Teflon at various strain rates are given in Figure 6.1. It can be interpreted from figure that experimental results of Teflon indicated similar characteristics against compressive loading. For comparison, maximum stress of 15 MPa was taken as the uppermost level of stress for quasi-static and SHPB tests. At the strain rate of 10^{-3} s^{-1}, maximum stress was reached at a strain around 0.8 while maximum strain was reduced to 0.1 at the strain rate of 9500 s^{-1} and depicted strong strain rate dependency. Densification strain was also found to be decreased with the increasing strain rate due to rapid stiffening behavior on Teflon with the increase in strain rate.

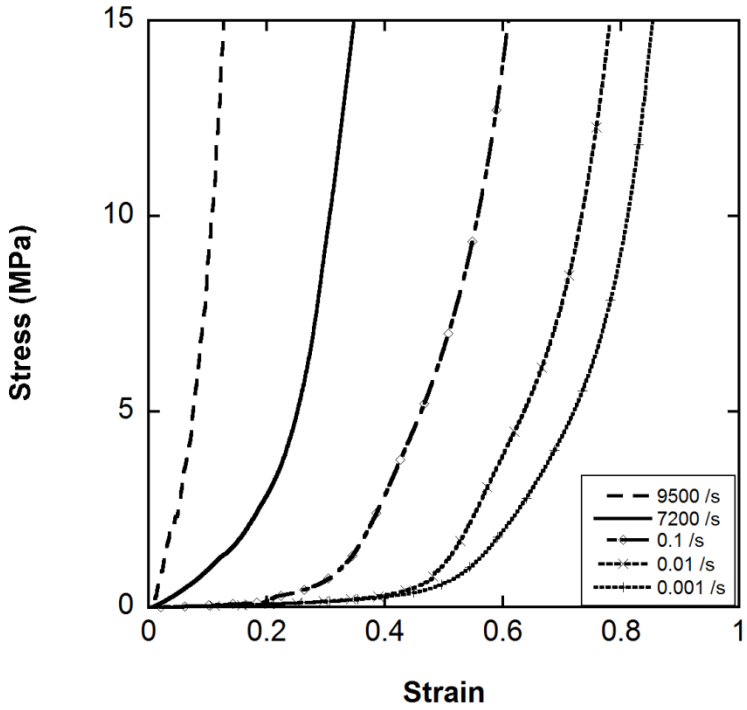

Figure 6.1. Comparison of experimental results of Teflon at various strain rates.

Compressive stress-strain curves of Polyurethane at various strain rates are given in Figure 6.2. Quasi-static tests were conducted at the strain rates of 10^{-3} s^{-1}, 10^{-2} s^{-1} and 10^{-1} s^{-1} whereas strain rates of 1360 s^{-1}, 1650 s^{-1} and 2260 s^{-1} were reached at SHPB tests. Quasi-static compression tests presented a linear region followed by plateau region with a small slope. Linear region in quasi-static regime nearly ended at the strain of 0.1 with same slope on each strain rate and modulus of elasticity was found to be around 46MPa. Between the strain of 0.1 and 0.2, stress-stain curves began to diverge. Finally, around the strain of 0.8, stress-strain curves can easily be distinguished, reaching the maximum stresses of 100 MPa, 95 MPa and 85 MPa with the increasing strain rate, respectively. For high strain rate regime, experimental results of Polyurethane displayed two linear regions with different slopes. Rapid compression of specimens in SHPB testing of polyurethane have resulted a sharp rise up to a strain of 0.1. Beyond the strain of 0.1, all of the stress-strain curves had a tendency to increase with a relatively smaller slope, reaching the final stress values of 42 MPa, 56 MPa and 107 MPa with the increasing strain rate, followed by unloading. In light of these consequences, experiments concluded strain rate dependency in Polyurethane and rate dependency is more pronounced with the increased strain levels.

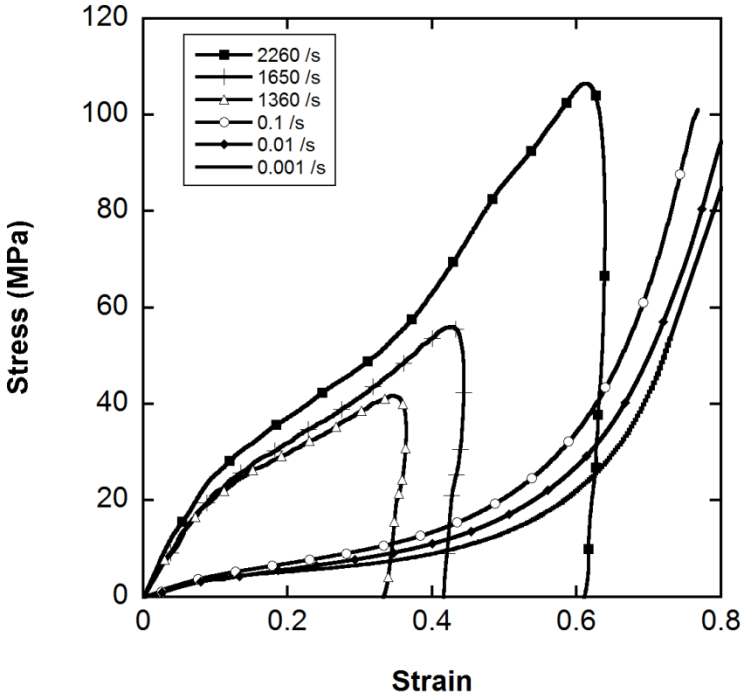

Figure 6.2. Comparison of experimental results of Polyurethane at various strain rates.

Numerical study focused on finite element modeling of SHPB experiments. Primary motivation is to verify the material model constants and to investigate the wave propagation inside material and dynamic deformation sequences; if numerical data, bar response, correspond well with experiment, material model constants can be further used in application of different impact events such as armor penetration. As stated before, Figure 5.8 and Figure 5.9 represent the comparison of bar responses and indicated a good correlation between numerical model and experimental results is noted. In addition, numerical model can provide additional information such as stress histories of specimen and force history of bars.

Figure 6.3 shows the comparison of transmitter bar force levels of Teflon both experimentally and numerically. Dashed line in Figure 6.3 represents experimental while solid line represents numerical. It can be seen from figure that experimental and numerical data do not correspond well up to 250 μs due to stress inequilibrium inside the specimen. This also verifies the necessity of quartz crystal usage during the tests. After 280 μs, experimental and numerical curves follow similar trend and greater correlation is observed up to 310 μs, which also shows the stress equilibrium.

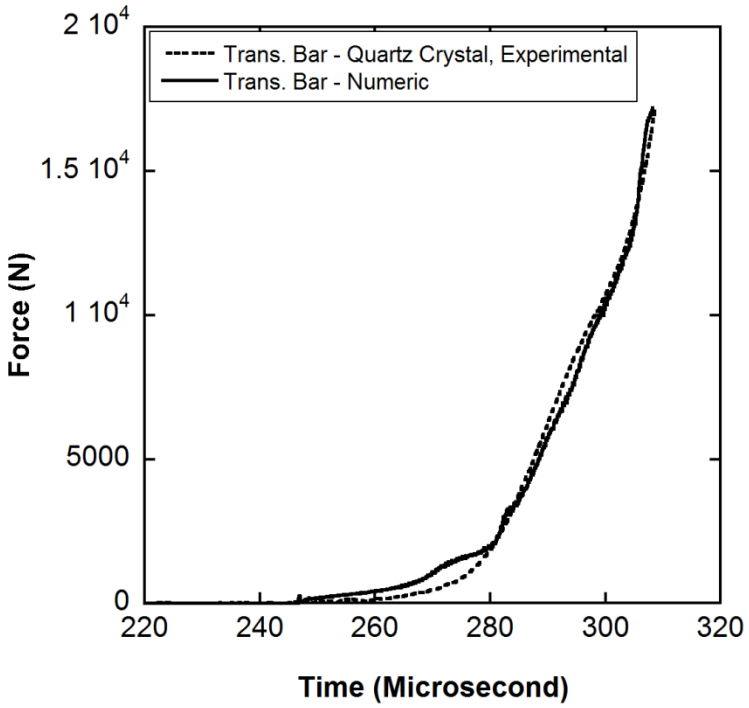

Figure 6.3. Comparison of experimental and numerical force levels on transmitter bar.

Comparison of axial force histories of front-end and back-end of specimen is given in Figure 6.4. Solid line in Figure 6.4 indicates the force history of front-end while force history of back-end is represented by dotted line. A slight deviation was observed between those curves during the loading phase while as the deformation continues, dynamic stress equilibrium was reached. However, front-end and back-end force histories do not match during unloading. In light of these consequences, it can be concluded that slight variations occur between front-end and back-end force histories during loading and unloading.

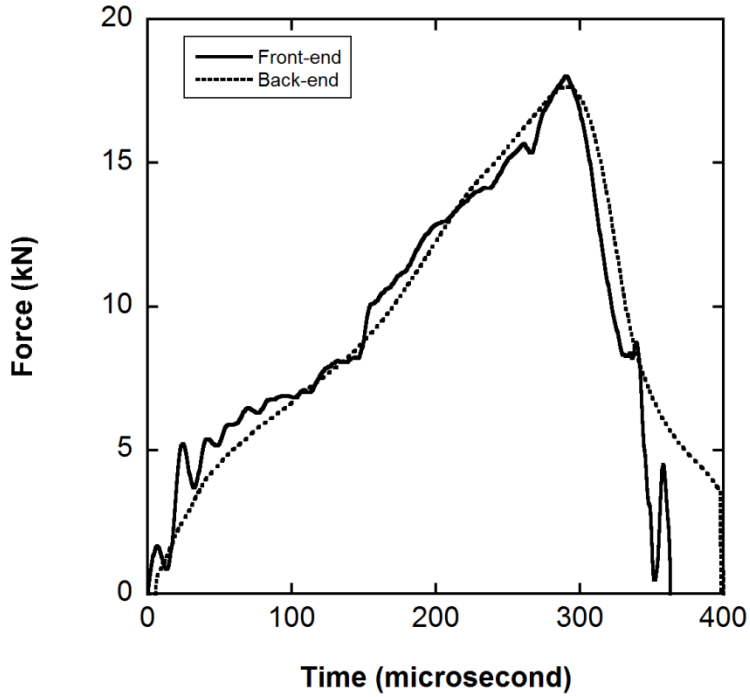

Figure 6.4. Force histories of front-end and back-end in Polyurethane sample.

Stress equilibrium in Split Hopkinson Pressure Bar experiments can be checked with dimensionless R parameter defined in Equation 2.5. Figure 6.5 indicates the variation of numerical R parameter with strain at the strain rate of 7200 s^{-1}. As seen in Figure 6.4, R converges to zero around strain of 0.4 after which stress equilibrium is reached in specimen.

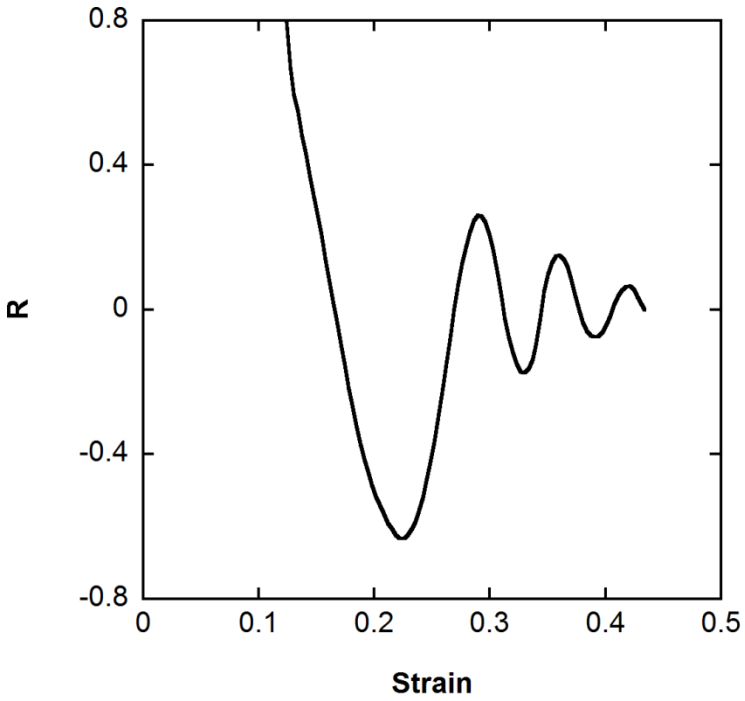

Figure 6.5. Dimensionless numerical R parameter-strain graph of Teflon.

Force equilibrium in finite element model of Polyurethane was also investigated and R parameter-strain graph at 1360 s^{-1} is given in Figure 6.6. It can be interpreted from the figure that the value of R converges from 1.5 to 0 about a strain of 0.18, indicating stress equilibrium is reached.

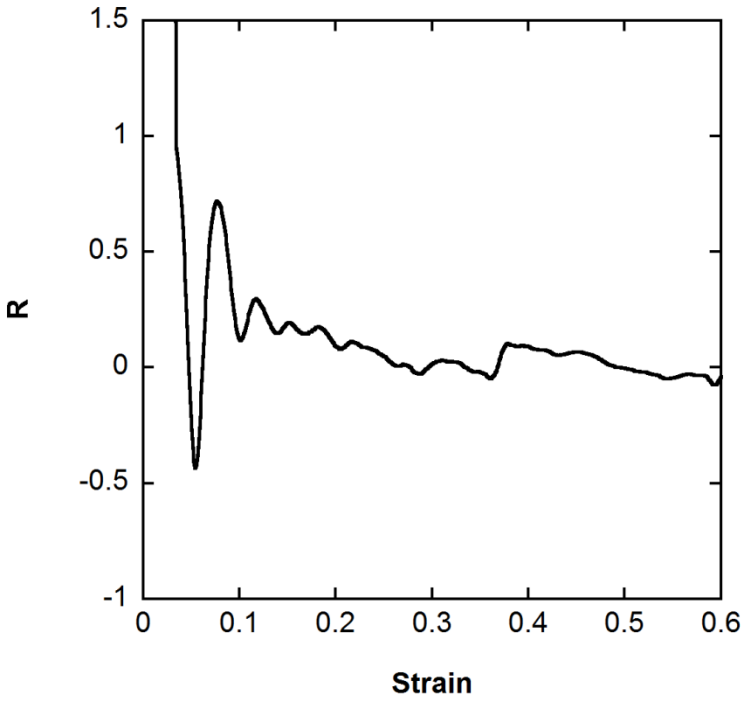

Figure 6.6. Dimensionless R parameter-strain graph of Polyurethane.

Real time damage behavior of Teflon during a SHPB test at 9500 s^{-1} was monitored at 10800 fps and comparison of experimental and numerical deformation profiles at three different time steps, 0 μs, 92 μs and 184 μs were given in Figure 6.7. The first row in Figure 6.7 represents the non-deformed specimens in both numerical and experimental study (0 μs). At 92 μs, while stress wave propagated through incident bar, specimen was compressed between incident and transmitter bars and expanded radially. At 184 μs, the last row of Figure 6.7, Teflon was fully compressed and tended to lose shape completely while being smeared on incident and transmitter bar interfaces. It can be concluded from the figure that mechanical behavior of Teflon is well duplicated in numerical model. A Teflon specimen before and after SHPB test is given in Figure 6.8.

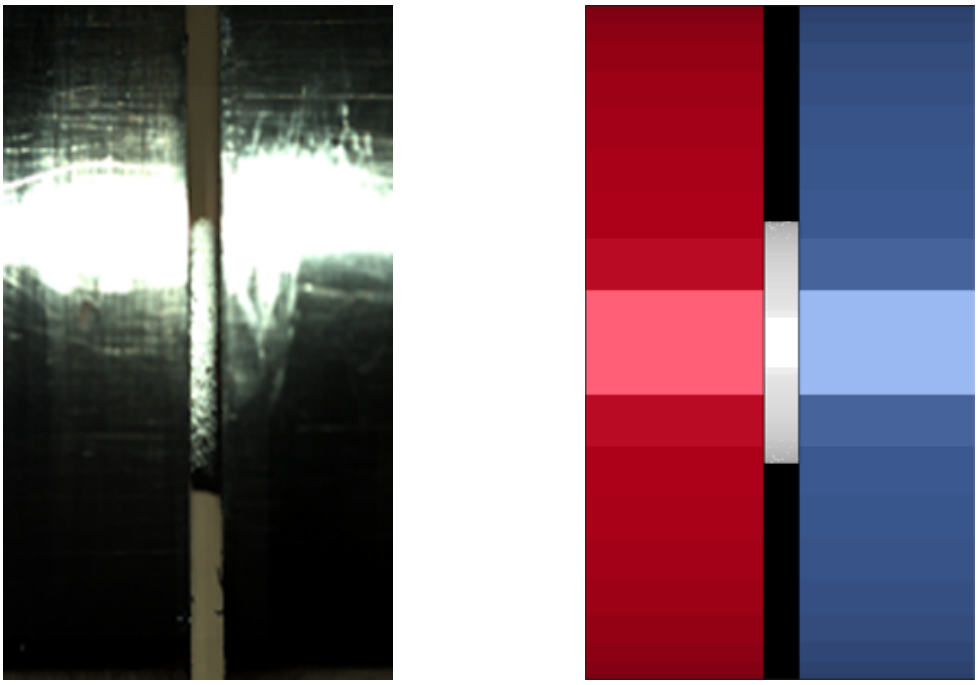

0 μs

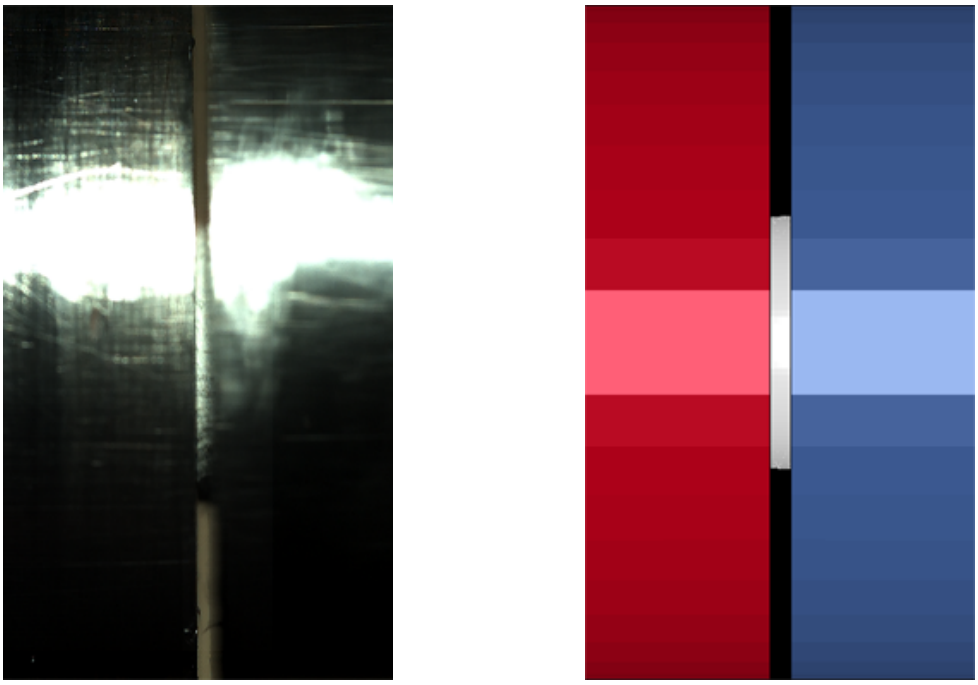

92 μs

Figure 6.7. Comparison of damage behaviors of Teflon a) experiment,
b) numerical model.

(cont. on next page)

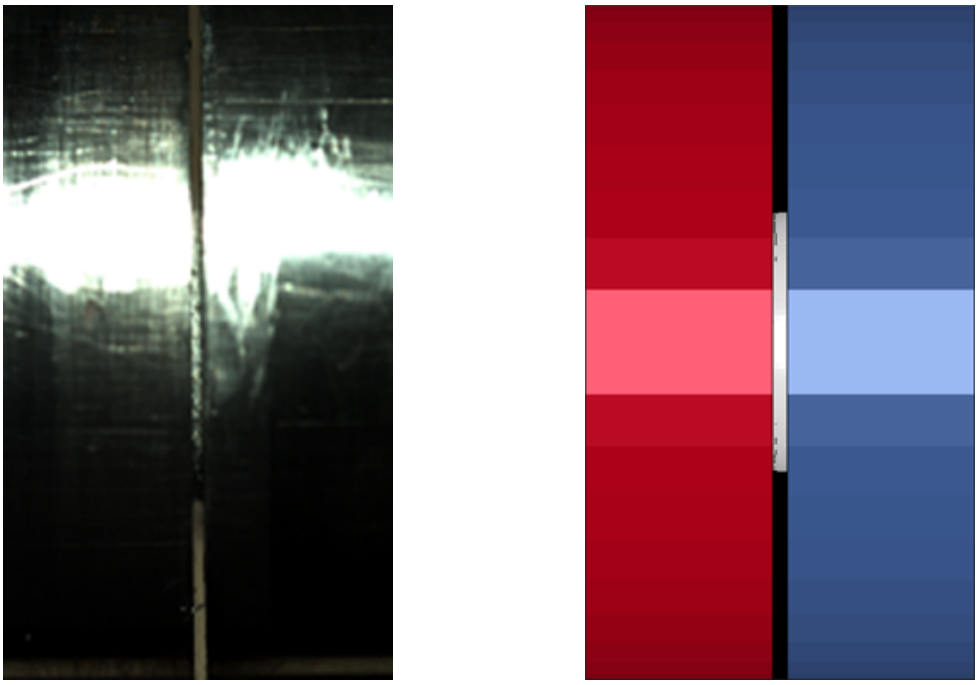

184 µs

a) b)

Figure 6.7. (cont.).

Figure 6.8. A Teflon specimen before and after an SHPB test.

Real time deformation behavior of Polyurethane at the strain rate of 1360 s^{-1} was recorded using high speed camera at 22500 fps during the SHPB test and recorded images were compared with those of numerical study in Figure 6.9. The first row of images represents the non-compressed samples in experimental and numerical studies (0 μs). As the stress wave traveled down the incident bar, specimens were compressed down to intermediate strain levels (44 μs). At 132 μs, as the strain was increased, Polyurethane was compressed and expanded radially while the length was reduced. No visible damage was observed through the experimental and numerical studies. Comparison of damage in Polyurethane specimen is given in Figure 6.10.

0 μs

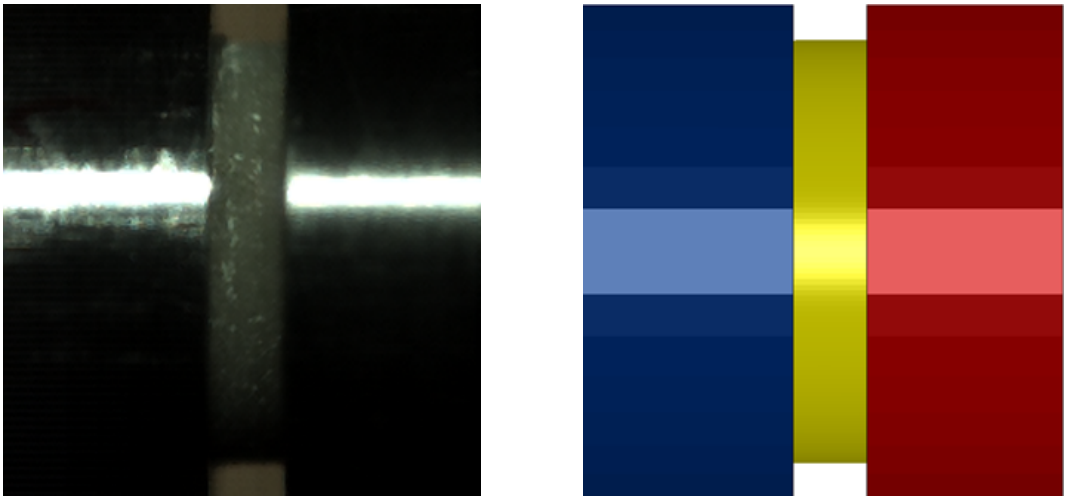

44 μs

Figure 6.9. Comparison of damage behaviors of Polyurethane a) experiment, b) numerical model.

(cont. on next page)

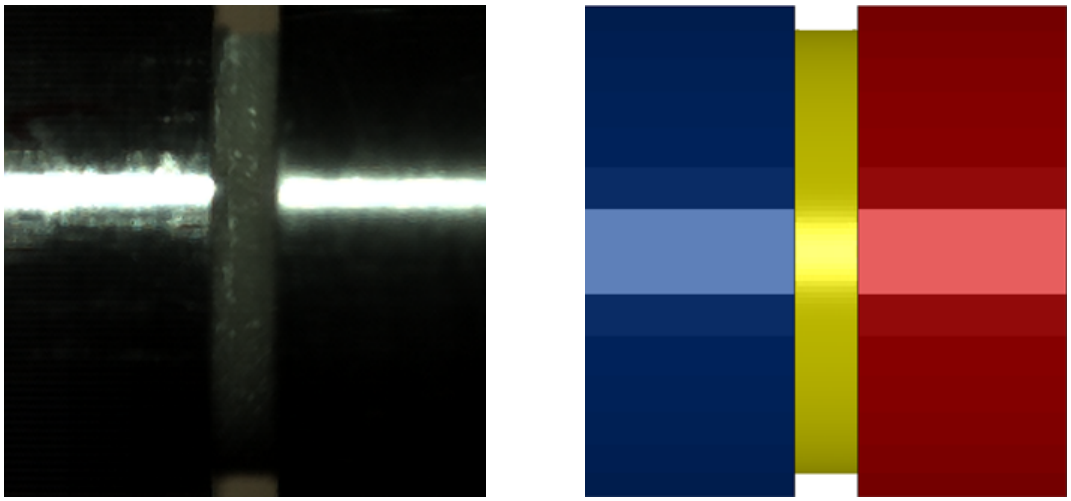

195 μs

a) b)

Figure 6.9. (cont.).

Figure 6.10. A Polyurethane specimen before and after an SHPB test.

CHAPTER 7

CONCLUSIONS

In this study, Gore™ Polarchip™ heat insulating Teflon and Dow Chemicals™ Voracor CS Polyurethane were characterized by conducting experiments at both quasi-static and high strain rates. Quasi-static tests were carried out using Shimadzu AG-X conventional test machine while SHPB set-up was used for high strain rate tests. During the high strain rate testing of Teflon, a quartz crystal implemented aluminum SHPB was used in order to minimize the problems associated with acoustic impedance mismatch between the bars and specimen. For SHPB testing of Polyurethane, steel bars along with pulse shapers were used. Pulse shaping reduced the oscillations occurring in input and output bar responses. Real time deformation of Teflon and Polyurethane was also recorded with a high speed camera.

After mechanical characterization, appropriate material models and their parameters were determined. SHPB tests were modeled using LS-DYNA 971 and material model parameters were checked by comparing experimental and numerical results. For both materials, crushable foam material model was successfully used. This well verified material can then be further used in the simulation of more complex impact problems such as armor penetration.

Experimental and numerical study revealed the following conclusions;

- Teflon indicated strong strain rate dependency. Quasi-static test results involved linear, plateau and densification regions, while a linear region followed by densification in SHPB tests.
- Strain rate dependency was also observed for Polyurethane. Quasi-static tests depicted linear, plateau and densification regions, while SHPB tests indicated two linear regions with different slopes.
- A well verified set of constants for each material was determined. Numerical results also confirmed the necessity of quartz crystal usage in SHPB testing of Teflon. Stress equilibrium was reached at low strain levels in SHPB testing of Polyurethane. Numerical deformation behaviors were also in accordance with those of experimental.

For the future work, these well verified material model parameters can further be used in simulating more complex problems such as penetration of armors containing these interlayers. These simulations can shed into light to the optimization of multilayered armor systems.

REFERENCES

[1] B. R. Sorensen, K. D. Kimsey, G. F. Silsby, D. R. Scheffler, T. M. Sherrick, and W. S. de Rosset, "High velocity penetration of steel targets," *International Journal of Impact Engineering,* vol. 11, pp. 107-119, 1991.

[2] D. L. Littlefield, C. E. Anderson Jr, Y. Partom, and S. J. Bless, "The penetration of steel targets finite in radial extent," *International Journal of Impact Engineering,* vol. 19, pp. 49-62, 1997.

[3] T. Børvik, M. Langseth, O. S. Hopperstad, and K. A. Malo, "Ballistic penetration of steel plates," *International Journal of Impact Engineering,* vol. 22, pp. 855-886, 1999.

[4] S. Sadanandan and J. G. Hetherington, "Characterisation of ceramic/steel and ceramic/aluminium armours subjected to oblique impact," *International Journal of Impact Engineering,* vol. 19, pp. 811-819, 1997.

[5] J. López-Puente, A. Arias, R. Zaera, and C. Navarro, "The effect of the thickness of the adhesive layer on the ballistic limit of ceramic/metal armours. An experimental and numerical study," *International Journal of Impact Engineering,* vol. 32, pp. 321-336, 2005.

[6] B. A. Roeder and C. T. Sun, "Dynamic penetration of alumina/aluminum laminates: experiments and modeling," *International Journal of Impact Engineering,* vol. 25, pp. 169-185, 2001.

[7] B. A. G. Gama, J. W., T. A. Bogetti, H. Mahfuz, and B. Fink, "Effect of non-linear material behavior on the through-thickness stress wave propagation in multi-layer hybrid lightweight armor," *Adv Comput Eng Sci Technol Sci Press,* pp. 157-62, 2000.

[8] B. A. Gama, T. A. Bogetti, B. K. Fink, C.-J. Yu, T. Dennis Claar, H. H. Eifert, and J. W. Gillespie Jr, "Aluminum foam integral armor: a new dimension in armor design," *Composite Structures,* vol. 52, pp. 381-395, 2001.

[9] B. A. G. Gama, J. W., T. A. Bogetti, and B. Fink, "Innovative design and ballistic performance of lightweight composite integral armor," presented at the SAE 2001 World Congress, Detroit, MI, 2001.

[10] A. Tasdemirci, G. Tunusoglu, and M. Güden, "The effect of the interlayer on the ballistic performance of ceramic/composite armors: Experimental and numerical study," *International Journal of Impact Engineering,* vol. 44, pp. 1-9, 2012.

[11] A. Tasdemirci, A. Kara, A. K. Turan, G. Tunusoglu, M. Guden, and I. W. Hall, "Experimental and Numerical Investigation of High Strain Rate Mechanical Behavior of a [0/45/90/ - 45] Quadriaxial E-Glass/Polyester Composite," *Procedia Engineering,* vol. 10, pp. 3068-3073, 2011.

[12] A. Tasdemirci and I. W. Hall, "Numerical and experimental studies of damage generation in multi-layer composite materials at high strain rates," *International Journal of Impact Engineering,* vol. 34, pp. 189-204, 2007.

[13] A. Tasdemirci and I. W. Hall, "The effects of plastic deformation on stress wave propagation in multi-layer materials," *International Journal of Impact Engineering,* vol. 34, pp. 1797-1813, 2007.

[14] A. Tasdemirci and I. W. Hall, "Development of novel multilayer materials for impact applications: A combined numerical and experimental approach," *Materials & Design,* vol. 30, pp. 1533-1541, 2009.

[15] W. Chen, F. Lu, and B. Zhou, "A quartz-crystal-embedded split Hopkinson pressure bar for soft materials," *Experimental Mechanics,* vol. 40, pp. 1-6, 2000.

[16] W. Chen, F. Lu, and N. Winfree, "High-strain-rate compressive behavior of a rigid polyurethane foam with various densities," *Experimental Mechanics,* vol. 42, pp. 65-73, 2002.

[17] B. Song, W. Chen, and D. J. Frew, "Dynamic Compressive Response and Failure Behavior of an Epoxy Syntactic Foam," *Journal of Composite Materials,* vol. 38, pp. 915-936, 2004.

[18] B. Song, "Strain-rate effects on elastic and early cell-collapse responses of a polystyrene foam," *International Journal of Impact Engineering,* vol. 31, pp. 509-521, 2005.

[19] S. Ouellet, D. Cronin, and M. Worswick, "Compressive response of polymeric foams under quasi-static, medium and high strain rate conditions," *Polymer Testing,* vol. 25, pp. 731-743, 2006.

[20] B. Song, W. Chen, Z. Liu, and S. Erhan, "Compressive properties of epoxidized soybean oil/clay nanocomposites," *International Journal of Plasticity,* vol. 22, pp. 1549-1568, 2006.

[21] G. Subhash, Q. Liu, and X. Gao, "Quasistatic and high strain rate uniaxial compressive response of polymeric structural foams," *International Journal of Impact Engineering,* vol. 32, pp. 1113-1126, 2006.

[22] A. Bryson and L. Smith, "Impact response of sports materials," *Procedia Engineering,* vol. 2, pp. 2961-2966, 2010.

[23] J. Yi, M. C. Boyce, G. F. Lee, and E. Balizer, "Large deformation rate-dependent stress–strain behavior of polyurea and polyurethanes," *Polymer,* vol. 47, pp. 319-329, 2006.

[24] S. S. Sarva, S. Deschanel, M. C. Boyce, and W. Chen, "Stress–strain behavior of a polyurea and a polyurethane from low to high strain rates," *Polymer,* vol. 48, pp. 2208-2213, 2007.

[25] J. Shim and D. Mohr, "Using split Hopkinson pressure bars to perform large strain compression tests on polyurea at low, intermediate and high strain rates," *International Journal of Impact Engineering*, vol. 36, pp. 1116-1127, 2009.

[26] B. Song, W. Chen, Y. Ge, and T. Weerasooriya, "Dynamic and quasi-static compressive response of porcine muscle," *J Biomech*, vol. 40, pp. 2999-3005, 2007.

[27] H. Luo, C. Dai, R. Z. Gan, and H. Lu, "Measurement of young's modulus of human tympanic membrane at high strain rates," *J Biomech Eng*, vol. 131, p. 064501, Jun 2009.

[28] F. Pervin, W. W. Chen, and T. Weerasooriya, "Dynamic compressive response of bovine liver tissues," *J Mech Behav Biomed Mater*, vol. 4, pp. 76-84, Jan 2011.

[29] H. Saraf, K. T. Ramesh, A. M. Lennon, A. C. Merkle, and J. C. Roberts, "Mechanical properties of soft human tissues under dynamic loading," *J Biomech*, vol. 40, pp. 1960-7, 2007.

[30] H. Zhao, G. Gary, and J. R. Klepaczko, "On the use of a viscoelastic split hopkinson pressure bar," *International Journal of Impact Engineering*, vol. 19, pp. 319-330, 1997.

[31] L. Wang, K. Labibes, Z. Azari, and G. Pluvinage, "Generalization of split Hopkinson bar technique to use viscoelastic bars," *International Journal of Impact Engineering*, vol. 15, pp. 669-686, 1994.

[32] W. Chen, B. Zhang, and M. Forrestal, "A split Hopkinson bar technique for low-impedance materials," *Experimental Mechanics*, vol. 39, pp. 81-85, 1999.